AD-A108 753 AIR FORCE WRIGHT AERONAUTICAL LABS WRIGHT-PATTERSON AFB OH F/G 20/11
A COMPILATION OF STRESS INTENSITY FACTOR SOLUTIONS FOR FLAWED F--ETC(U)
NOV 81 A F GRANDT, T E KULLGREN
UNCLASSIFIED AFWAL-TR-81-4112 NL

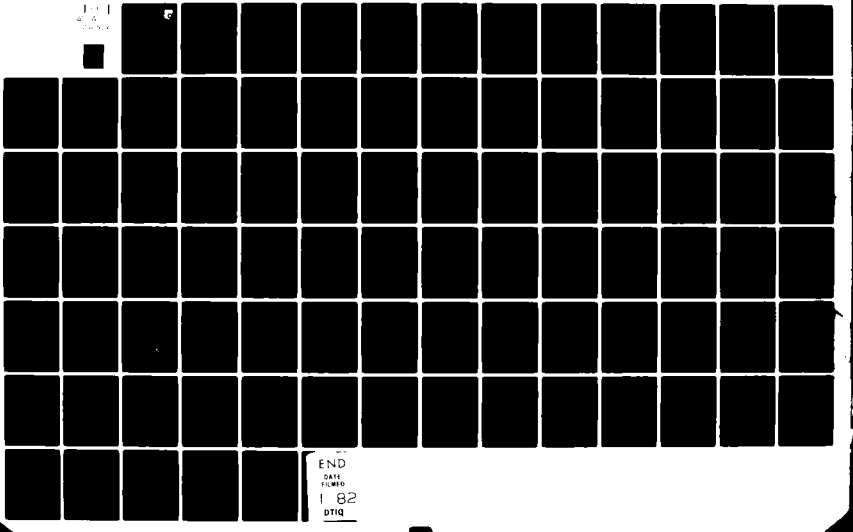

END
DATE FILMED
1 82
DTIC

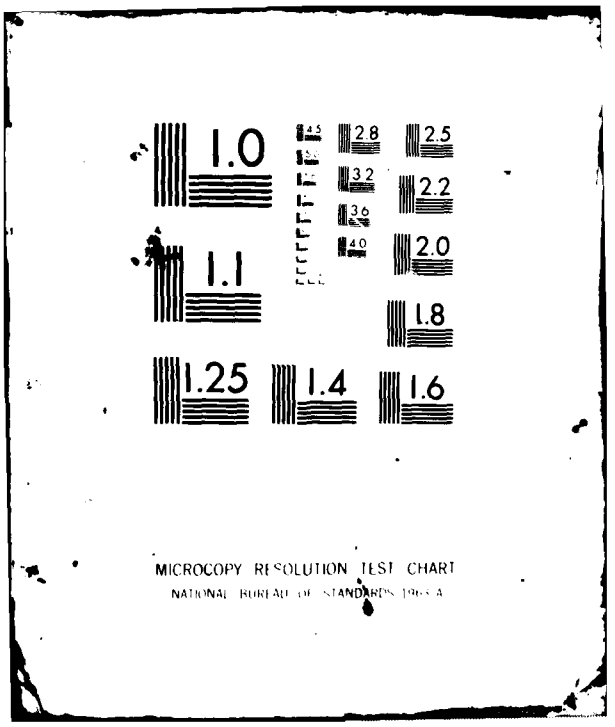
1.0
1.1
1.25
1.4
1.6
2.8
3.2
3.6
4.0
2.5
2.2
2.0
1.8
MICROCOPY RESOLUTION TEST CHART
NATIONAL BUREAU OF STANDARDS 1963-A

AFWAL-TR-81-4112

A COMPILATION OF STRESS INTENSITY FACTOR SOLUTIONS FOR FLAWED FASTENER HOLES

A. F. Grandt, Jr.
School of Aeronautics & Astronautics
Purdue University
W. Lafayette, Indiana 47907

T. E. Kullgren
Department of Engineering Mechanics
USAF Academy, Colorado 80840

November 1981
Final Report for Period June 1978 to August 1981

Approved for public release; distribution unlimited

MATERIALS LABORATORY
AIR FORCE WRIGHT AERONAUTICAL LABORATORIES
AIR FORCE SYSTEMS COMMAND
WRIGHT-PATTERSON AIR FORCE BASE, OHIO 45433

NOTICE

When Government drawings, specifications, or other data are used for any purpose other than in connection with a definitely related Government procurement operation, the United States Government thereby incurs no responsibility nor any obligation whatsoever; and the fact that the government may have formulated, furnished, or in any way supplied the said drawings, specifications, or other data, is not to be regarded by implication or otherwise as in any manner licensing the holder or any other person or corporation, or conveying any rights or permission to manufacture use, or sell any patented invention that may in any way be related thereto.

This report has been reviewed by the Office of Public Affairs (ASD/PA) and is releasable to the National Technical Information Service (NTIS). At NTIS, it will be available to the general public, including foreign nations.

This technical report has been reviewed and is approved for publication.

THEODORE NICHOLAS
Project Engineer
Metals Behavior Branch

FOR THE COMMANDER

JOHN P. HENDERSON, Chief
Metals Behavior Branch
Metals and Ceramics Division

"If your address has changed, if you wish to be removed from our mailing list, or if the addressee is no longer employed by your organization please notify AFWAL/MLLN, W-PAFB, OH 45433 to help us maintain a current mailing list".

Copies of this report should not be returned unless return is required by security considerations, contractual obligations, or notice on a specific document.

AIR FORCE/56780/11 December 1981 — 600

UNCLASSIFIED

SECURITY CLASSIFICATION OF THIS PAGE (When Data Entered)

REPORT DOCUMENTATION PAGE		READ INSTRUCTIONS BEFORE COMPLETING FORM
1. REPORT NUMBER AFWAL-TR-81-4112	2. GOVT ACCESSION NO. AD-A108	3. RECIPIENT'S CATALOG NUMBER 753
4. TITLE (and Subtitle) A COMPILATION OF STRESS INTENSITY FACTOR SOLUTIONS FOR FLAWED FASTENER HOLES		5. TYPE OF REPORT & PERIOD COVERED Final report June 1978 - August 1981 6. PERFORMING ORG. REPORT NUMBER
7. AUTHOR(s) *A. F. Grandt, Jr. **T. E. Kullgren		8. CONTRACT OR GRANT NUMBER(s)
9. PERFORMING ORGANIZATION NAME AND ADDRESS Materials Laboratory(AFWAL/MLLN, MLSA) Air Force Wright Aeronautical Laboratories Wright-Patterson AFB, OH 45433		10. PROGRAM ELEMENT, PROJECT, TASK AREA & WORK UNIT NUMBERS 2307P102 2418
11. CONTROLLING OFFICE NAME AND ADDRESS Materials Laboratory (AFWAL/MLL, MLS) Air Force Wright Aeronautical Laboratories Wright-Patterson Air Force Base, Ohio 45433		12. REPORT DATE November 1981 13. NUMBER OF PAGES 86
14. MONITORING AGENCY NAME & ADDRESS(if different from Controlling Office)		15. SECURITY CLASS. (of this report) UNCLASSIFIED 15a. DECLASSIFICATION/DOWNGRADING SCHEDULE

16. DISTRIBUTION STATEMENT (of this Report)

Approved for public release, distribution unlimited.

17. DISTRIBUTION STATEMENT (of the abstract entered in Block 20, if different from Report)

18. SUPPLEMENTARY NOTES

*School of Aeronautics & Astronautics
Purdue University
W. Lafayette, Indiana 47907

**Department of Engineering Mechanics
USAF Academy, Colorado 80840

19. KEY WORDS (Continue on reverse side if necessary and identify by block number)

Stress intensity factor
Fracture mechanics
Fastener holes
Flaws

20. ABSTRACT (Continue on reverse side if necessary and identify by block number)

Several sets of stress intensity factor solutions are provided for through-the-thickness, corner, and surface flawed holes. Results are given for both remote tensile and crack face pressure loading. It is suggested that the crack face pressure solutions can be used with the linear superposition method to analyze many other practical crack problems. The superposition technique is demonstrated with several sets of example calculations.

DD FORM 1 JAN 73 1473 EDITION OF 1 NOV 65 IS OBSOLETE

UNCLASSIFIED

SECURITY CLASSIFICATION OF THIS PAGE (When Data Entered)

FOREWORD

This report was prepared by the Metals Behavior Branch, Metals and Ceramics Division, and the Materials Integrity Branch, Systems Support Division, Materials Laboratory, Air Force Wright Aeronautical Laboratories, Wright-Patterson Air Force Base, Ohio. The research reported herein was conducted, in part, under Project No. 2307, "Solid Mechanics", Task 2307P1, "Life Prediction and Failure Mechanisms", and under Project 2418, "Metallic Applications." Portions of this research were conducted by the first author while he was associated with the Materials Laboratory. This work was performed during the period June 1978 to August 1981.

The authors are indebted to the continuing interest and support provided by T. Nicholas and C. L. Harmsworth of the Materials Laboratory and greatly appreciate the computer support provided by G. Griffin of the University of Dayton Research Institute. The support of the Department of Engineering Mechanics, USAFA, in providing time for the second author to conduct this research, is gratefully acknowledged.

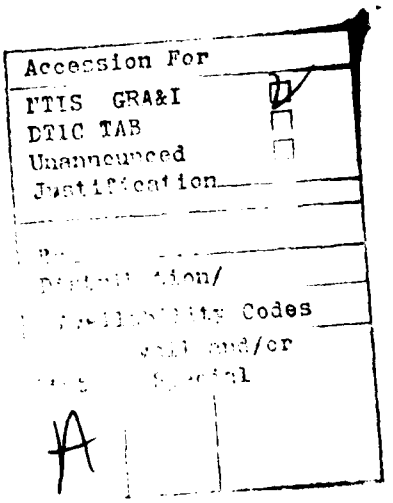

TABLE OF CONTENTS

Table of Contents(cont'd)

LIST OF TABLES

List of Tables (cont'd)

LIST OF FIGURES

SECTION I

INTRODUCTION

BACKGROUND

The objective of this report is to present a set of "general" stress intensity factor solutions for several cracked hole configurations. As described later, the crack surfaces are loaded with an arbitrary crack face pressure in a manner which allows the results to be applied to many other practical loading conditions. Solutions are given for the through-the-thickness, corner, and surface cracked hole geometries shown schematically in Figure 1.

It is commonly known that such cracks often originate at fastener holes in mechanically fastened joints, and may represent a failure source for aircraft structures. The United States Air Force, for example, has adopted fracture mechanics based design criteria which require new aircraft to resist failure from pre-existent cracks assumed present at fastener holes (1). Such analyses require stress intensity factor (K_I) solutions for the assumed flaw geometry. Since the fastener hole can be subjected to a variety of complex loadings, many different stress intensity factor solutions may be required. In addition to varying degrees of load transfer through the fastener, for example, residual stresses may be introduced around the hole (by coldworking or by use of interference fit fasteners) to improve the joint fatigue life (2-4). The loading conditions may be further complicated by bending, thermal, or dynamic effects.

This report describes a series of "crack face pressure" stress intensity factor solutions which may be readily applied to a wide variety of such loading conditions. The remainder of this section overviews the superposition techn ;ue which :ovides the general utility for the crack face pressure

solutions presented here. Subsequent sections describe the analysis techniques used to obtain the crack face pressure solutions, discuss the results, and demonstrate their application through several example problems.

LINEAR SUPERPOSITION

In order to describe the nature of the crack face pressure stress intensity factors, and demonstrate their generality, the well known linear superposition procedure shown schematically in Figures 2 and 3 will be briefly reviewed. As indicated in Figure 2, a cracked body subjected to arbitrary elastic loading (member A) can be resolved into two components (B and C). Member B consists of the uncracked geometry loaded as in case A. A stress free line is introduced along the desired crack plane by canceling the resulting hoop stress through application of $-p(x/R)$. Here x is the distance measured from the edge of the hole (its radius is R) and $p(x/R)$ is the hoop stress distribution along the crack plane caused by loading the unflawed member. Since the crack plane is now stress free, a crack can be introduced. Member C consists of the cracked body loaded along the crack faces with the pressure $+p(x/R)$. By superposition, the stress intensity factor for member A is the linear sum of the stress intensity factors for members B and C.

$$K_A = K_B + K_C \tag{1}$$

Now, since the crack plane in member B is stress free, $K_B = 0$, and $K_A = K_C$. Thus, the stress intensity factor for the original problem is identical to that for a crack loaded with the unflawed hoop stress distribution.

If the crack face pressure is defined in terms of a polynomial expansion, it is possible to obtain a "general" solution in terms of the polynomial coefficients. This latter point is demonstrated by the superposition described in Figure 3, where

$$p(x/R) = A_0 + A_1(x/R) + A_2(x/R)^2 + \ldots \tag{2}$$

Here the crack face pressure is expressed in terms of the dimensionless

distance x/R from the edge of the hole, and the A_n (n = 0, 1, 2, ...) are the polynomial coefficients determined for the unflawed hoop stress distribution (the A_n have units of stress). Note that the stress intensity factors for the cracks shown in Figure 3 are again linearly superimposed.

$$K_I = K_0 + K_1 + K_2 + \ldots = \Sigma K_n \tag{3}$$

Here K_I is the mode-one stress intensity factor for the complete crack face loading (equivalent to the original stress intensity factor for member A in Figure 2), and the K_n are the stress intensity factors due to the individual pressure terms $A_n(x/R)^n$ in the expansion for $p(x/R)$.

Note that if the K_n are obtained for arbitrary polynomial coefficients A_n, and are expressed in the dimensionless form given by Eq. 4, the results are readily applied to other plate loadings.

$$M_n = \frac{K_n}{A_n \sqrt{\pi c}} \tag{4}$$

Here the magnification factor M_n is defined for each individual term in the crack face pressure expansion and c is the crack length measured in the radial direction. Now, given the A_n and crack length for the new problem of interest, the desired stress intensity factor K_I is found from the general results (the M_n) by performing the summation of Eq. 3.

$$K_I = \Sigma K_n = \sqrt{\pi c} \sum^{\nu} \frac{K_n}{A_n \sqrt{\pi c}} A_n \tag{5}$$

$$= \sqrt{\pi c}\, \Sigma M_n A_n = K_I$$

Thus, the magnification factors M_n obtained for the crack face pressure loading represent general solutions which may be used to compute stress intensity factors for any loading once the unflawed hoop stress is found and represented by Eq. 2. Note that although the hoop stress must still be determined for the unflawed fastener hole problem of interest, the fact that the cracked hole does not have to be directly analyzed greatly

simplifies computational effort. It is anticipated that the unflawed problem will be analyzed by a conventional stress analysis method (e.g. finite elements).

This general analysis procedure is demonstrated in subsequent sections by several example calculations with through-the-thickness, quarter-elliptical, and semielliptical fastener hole cracks. These examples employ results given here for the dimensionless crack face pressure stress intensity factor M_n. Prior to discussing those results, however, the analysis procedures used to obtain the crack face pressure solutions (the K_n and subsequently M_n) are described.

SECTION II

CRACK FACE PRESSURE ANALYSIS METHODS

This section describes the analysis procedures used to obtain the general crack face pressure solutions for the two-dimensional through-the-thickness and the three-dimensional corner- and surface-cracked hole configurations. A weight function approach was used for the through-the-thickness cracks, while the finite element - alternating method was employed for the quarter- and semielliptical cracks.

THROUGH-THE-THICKNESS CRACKS

The through-cracked hole problem is shown in Figure 4. An earlier solution (5) developed for the arbitrary crack face pressure loading was used to compute K_n for the individual pressure term $A_n(x/R)^n$. As described in Reference 5, weight function methods allowed computation of the crack face pressure solution from stress intensity factor (6) and crack opening displacement results for remote tensile loading.

The crack face pressure solution obtained by the weight function method is given by

$$K_I = \frac{H}{K^*} \int_0^c p(x/R) \frac{\partial \eta}{\partial c} dx \qquad (6)$$

Here K* is the stress intensity factor for remote tensile loading applied perpendicular to the crack plane (6), c is the crack length, R is the hole radius, η is the crack opening displacement profile corresponding to K*, p(x/R) is the crack face pressure as before, and H is a material constant defined in terms of the elastic modulus and Poisson's ratio. A procedure for computing the derivative of the crack opening profile with respect to crack length $(\frac{\partial \eta}{\partial c})$ is described in Reference 5. A computer program was employed to numerically integrate Eq. 6 for the crack face pressure loading p(x/R) defined by Eq. 2. Calculations reported

in References 4 and 5 indicate that the stress intensity factor solutions obtained by applying Eq. 6 with the linear superposition procedure outlined earlier in conjunction with Figure 2 give excellent stress intensity factor results when the unflawed hoop stress distribution is used to define the crack face pressure solution. Thus, based on this successful experience with the arbitrary crack face pressure solution, Eq. 6 was used to compute K_n (and the dimensionless magnification factor M_n) for the crack face loading $A_n (x/R)^n$. These results for M_n are summarized in a later section of this report.

CORNER AND SURFACE CRACKS

The quarter-elliptical and semielliptical surface cracks located at the fastener holes are shown in Figures 5 and 6. Here T is the plate thickness, R is the hole radius, a is the semiaxis of the elliptical crack boundary measured along the bore of the hole, c is the semiaxis length in the radial direction, and ϕ is the "parametric" angle which defines points along the border of a circle circumscribed around the part elliptical crack. A projection from the circle defines points along the crack border. The x and z coordinates (see Figures 5 and 6) of points along the crack perimeter are given by $x = c \cos \phi$ and $z = a \sin \phi$.

The finite element - alternating method was used to obtain the stress intensity factor variation around the perimeter of the corner- and surface-cracked holes. The finite element - alternating method was developed by F. W. Smith and his associates and has been successfully applied to several surface crack problems (7-10). Specific use was made here of computer codes developed by Smith and Kullgren for the analyses described in Reference 10.

The finite element - alternating method involves iterative superposition of a three-dimensional finite element solution for an uncracked body subjected to a prescribed surface loading (11) and a solution for a flat elliptical

crack in an infinite body loaded with a prescribed nonuniform surface pressure (12). Iteration between these two solutions approximates the surface crack boundary conditions and provides mode-one stress intensity factors and crack opening displacements for the three-dimensional flaw geometry. Additional details of the finite element - alternating method are presented in References 7-10.

Comparisons of stress intensity factors obtained by the finite element - alternating procedure with other experimental and numerical solutions for cracked fastener holes indicate that the analysis method provides excellent stress intensity factor results for this class of problem. Kullgren and Smith (8-10), for example, have applied the finite element - alternating method to a series of surface-cracked holes in large plates. Results are presented for three crack locations near fastener holes in plates with two hole diameter to plate thickness ratios. Plate loading conditions included remote uniaxial tension and 100 percent transfer of load to a fastener filled hole. Those results have been verified in several ways. Three-dimensional calculations (8-10) by the finite element - alternating method for through-cracked holes loaded in remote tension agree within 3.2 percent for single crack results reported by Tweed and Rooke (13) and within 5 percent of Bowie's double flaw solution (6). Corner crack results agree to within about 10 percent of finite element data reported by Raju and Newman (14). Other favorable comparisons of the finite element - alternating method are reported in Reference 10 for experimental data obtained for static fracture (15) and fatigue crack growth tests (16) with corner-cracked holes. A more recent study (17) involving simulated aircraft spectrum loading with 2124-T851 aluminum specimens indicated that stress intensity factors obtained by the current analysis accurately predict fatigue crack growth life and changes in crack shape.

In view of this prior success with the finite element - alternating method, this analysis technique was used to determine the crack face pressure stress intensity factor solutions for the corner- and surface-cracked holes. Those results, along with the through-cracked hole data obtained by the weight function method are discussed in the following section.

SECTION III

STRESS INTENSITY FACTOR RESULTS

The objective of this section is to present the stress intensity factor solutions obtained for the flawed fastener holes. Application of these "general" crack face pressure results to several example problems are discussed in the following section.

THROUGH-CRACKED HOLES

As described earlier, a weight function method was used to compute stress intensity factors for through-cracked holes loaded with a crack face pressure $A_n (x/R)^n$. Seven individual pressure terms were considered as n varied in the range $0 \leq n \leq 6$. Although both single and double symmetric cracks were examined, the dimensionless crack lengths were restricted to the range $0.1 \leq c/R \leq 2.5$. The stress intensity factor results are summarized in the dimensionless form $M_n = K_n/(A_n\sqrt{\pi c})$ in Tables 1 and 2. These data, along with similar results for through-cracked rings, were reported earlier in Reference 18.

CORNER-CRACKED HOLES

The quarter-elliptical corner crack geometry is shown in Figure 5. The cracked hole problems considered here are summarized in Table 3. In all cases, the plate hole diameter to thickness ratio 2R/T was fixed at 1.0, Poisson's ratio was kept at a value of 0.25, and the "large" circular plate had an outer radius = 12 R.

Although solutions for a large matrix of crack shapes would be desirable, the alternating method requires fairly large computer costs. Thus, care was taken to select the problems considered. The USAF damage tolerance specifications described in Reference 1 require analysis of quarter circular corner cracks (a/c = 1.0). As discussed in Reference 10, however, the

computer codes employed by the present authors have a numerical instability at a/c = 1.0. Although this instability is associated with the computer programming, and has no physical significance, it prevented direct analysis of quarter circular corner cracks. Thus, aspect ratios a/c = 0.9 and 1.1 were selected to closely bracket the crack shapes specified in the USAF requirements. Emphasis was placed on results for a/c = 1.1 rather than 0.9 because experience indicates that naturally occurring fatigue cracks often have a/c values between 1.0 and 1.5 (16).

The loading conditions considered here included the first four individual terms in the polynomial expansion for the crack face pressure. Thus, n covered the range $0 \le n \le 3$ for the pressure distribution given by $A_n(x/R)^n$. Computations were also performed for a remote tensile stress σ applied perpendicular to the crack plane (see Figure 7).

The corner-cracked hole stress intensity factor results are summarized in Tables 4 and 5. Here the dimensionless magnification factor is presented as a function of crack shape (a/c), size (a/t), position along the crack front ϕ, and applied load. These results were presented earlier in Reference 19.

The magnification factor in Table 4 is defined by

$$M_n = \frac{K_n}{A_n\sqrt{\pi a}} \tag{7}$$

As described earlier, K_n is the stress intensity factor caused by $A_n(x/R)^n$ in the crack face pressure expansion defined by Eq. 2. Note that since the polynomial coefficients A_n have units of stress (see Eq. 2), the magnification factor M_n is dimensionless. The data in Table 4 are for values of n = 0, 1, 2, and 3.

The results in Table 5 are for a remote stress σ applied perpendicular

to the crack plane. Here the dimensionless magnification factor is given by

$$M_n = \frac{K_I}{\sigma \sqrt{\pi a}} \tag{8}$$

where K_I is the stress intensity factor caused by the remote stress σ. All of the results presented in Tables 4 and 5 are for a material having a Poisson's ratio of 0.25, a hole diameter to plate thickness ratio $2R/T = 1.0$ and are reported for 30 degree increments of the "parametric" angle ϕ defined in Figure 5.

In contrast to the crack face pressure results (Table 4), the remote stress (Table 5) data include through-the-thickness effects in the stress intensity factor calculations. Reference 20 discusses a three-dimensional stress analysis for remotely loaded holes in plates of arbitrary thickness, and indicates that the unflawed hoop stress for the geometry considered here (hole diameter = plate thickness) can vary by as much as 10 percent in the thickness direction (z direction in Figures 5 and 6) at the bore of the hole. As described in Reference 10, direct application of the finite element - alternating method to the remote load problem (the Table 5 results) takes this three-dimensional effect into account.

SURFACE-CRACKED HOLES

The semielliptical surface-cracked hole geometry is shown in Figure 6. The flaw shapes and loading conditions considered here are summarized in Table 6. The loading conditions again consisted of the individual crack face pressure terms $A_n(x/R)^n$ where $0 \le n \le 3$, and a remote tensile stress σ applied perpendicular to the crack plane as in Figure 7. Crack shapes include aspect ratios $a/c = 1.11$, 1.5, and 2.0 and crack lengths $2a/T = 0.2$, 0.4, 0.6, 0.8, and 1.0.

The crack shapes studied were selected to agree with those found to occur "naturally" for this flaw configuration. Experiments with surface-

cracked hole specimens loaded in remote tension reported by Kullgren and Smith (15), for example, gave crack shapes in the range of $2.17 \leq a/c \leq 1.52$ with a/c = 1.85 as the average value. Fractographic examination of cracked fastener holes in retired jet engine turbine disks reported in Reference 21 give typical aspect ratios on the order of a/c = 1.4. Specimens prepared for a nondestructive inspection study (22) associated with a recent damage tolerance analysis conducted on another USAF turbine engine gave small semi-elliptical cracks with aspect ratios in the range of $1.2 \leq a/c \leq 1.0$. Hsu et. al. (23) also report fatigue data for fastener holes with two symmetric surface cracks (one on each side of the hole) with aspect ratios $1.50 \leq a/c \leq 1.25$.

Dimensionless stress intensity factors for the two loading configurations (crack face pressure and remote stress) are presented in Tables 7 and 8 as a function of position along the crack perimeter (ϕ), crack size (2a/T), and flaw shape (a/c). Again the plate hole to thickness ratio 2R/T = 1.0, Poisson's ratio has a value of 0.25, and the remote stress loading results incorporate the same through-the-thickness variation in stress described earlier for the corner-cracked hole configuration. The magnification factors M_n and M are defined by

$$M_n = \frac{K_n}{A_n\sqrt{\pi c}} \tag{9}$$

and

$$M = \frac{K}{\sigma\sqrt{\pi c}} \tag{10}$$

These results are also reported in Reference 24. Note that the magnification factor for the semielliptical surface cracks (Eqs. 9 and 10) are defined with the dimension "c" in the denominator rather than "a" as used in Eqs. 7 and 8 for corner cracks.

STRESS FUNCTION COEFFICIENTS

Tables 4, 5, 7 and 8 present tabulated stress intensity factors for the corner and embedded (surface) cracks at 30° increments of the parametric angle ϕ. The original computer output gave results for other angles and also provided crack opening displacement information. Although a complete tabulation of all the available data is too voluminous for this report, it is possible to provide information which can be used to reconstruct both stress intensity factors and crack opening displacements for additional values of the parametric angle ϕ. Appendix A, for example, summarizes a set of 10 stress function coefficients which were computed (see Refs., 10 and 12 for details) for each crack configuration considered here. Computer programs described in Appendices B and C, use these stress function coefficients to recalculate stress intensity factors and crack opening displacements as a function of the parametric angle ϕ. Thus, as demonstrated in the appendices, the reader can readily obtain complete descriptions of stress intensity factors and crack opening displacements for all of the problems summarized in Tables 3 and 6. (These problems are relisted and numbered in Tables A-1 and A-2 of Appendix A.)

SECTION IV

EXAMPLE PROBLEMS

The purpose of this section is to demonstrate application of the "general" stress intensity factor solutions reported in Tables 1, 2, 4, and 7. These crack face pressure results are applied to several example problems in order to further explain the calculations of Eq. 5, and to indicate the general utility of the tabulated data. Where possible, these calculations are compared with independent results in order to assess the accuracy of the superposition procedure.

EXAMPLE 1: THROUGH-CRACKED HOLE LOADED IN REMOTE TENSION

This example demonstrates the use of crack face pressure results in Table 1 to compute the stress intensity factor for a through-cracked hole loaded in remote tension perpendicular to the crack plane. This flaw geometry was analyzed by Bowie (6) and stress intensity factor results are reported in Reference 25. For demonstration purposes, assume crack length $c = 0.5R$ and the applied stress is σ.

The first step in the computational procedure is to determine the unflawed hoop stress σ_H caused by the remote load. A two-dimensional stress analysis for σ_H is given in Reference 26. Least squares procedures were employed here to express that result in the polynomial expansion given by Eq. 2. The following expression agrees within three percent of the exact analysis for $0 \le x/R \le 1.0$, where σ is the remote stress.

$$\sigma_H = \sigma\left[2.9190 - 5.2853(x/R) + 6.2574(x/R)^2 - 2.6910(x/R)^3\right] \qquad (11)$$

Now, letting the crack face pressure $p(x/R) = \sigma_H$, the pressure polynomial

coefficients (A_n) and magnification factors (M_n) from Table 1 (for c/R = 0.5) are

$$A_0 = 2.9190\,\sigma \qquad M_0 = .9119$$
$$A_1 = -5.2853\,\sigma \qquad M_1 = .3020$$
$$A_2 = 6.2574\,\sigma \qquad M_2 = .1207$$
$$A_3 = -2.6910\,\sigma \qquad M_3 = .05167$$

The desired stress intensity factor is now given by Eq. 5 as

$$K_I = \sum_{n=0}^{3} K_n = \sqrt{\pi c}\sum \frac{A_n K_n}{A_n \sqrt{\pi c}} = \sqrt{\pi c}\ \sum A_n M_n$$

$$= \sigma\sqrt{\pi c}\ \left[(2.9190)(.9119) - (5.2853)(.3020) + (6.2574)(.1207) - (2.6910)(.05167)\right] = 1.6819\,\sigma\sqrt{\pi c} = K_I.$$

The corresponding result given in Reference 25 (for c/R = 0.5) is $K_I = 1.73\,\sigma\sqrt{\pi c}$. Thus, the solution obtained by the superposition procedure agrees within three percent of the "exact" result found by direct analysis (6) of the cracked member.

EXAMPLE 2: THROUGH-CRACKED COLDWORKED HOLE

Coldworking fastener holes is an effective method for extending the fatigue lives of mechanically fastened joints. The process involves introducing residual compressive hoop stresses at the hole edge by pulling an oversize mandrel through the hole. These residual stresses reduce the effective stress concentration when remote load is applied, and can greatly extend the fatigue life of fastener holes (2-4).

The purpose of this example is to demonstrate application of the tabulated crack face pressure solutions to the coldworking process. As discussed in Reference 4, consider a 0.261 inch (6.63 mm) diameter hole in a 0.261 inch

(6.63 mm) thick plate of 7075-T651 aluminum. A 0.274 inch (6.96 mm) diameter mandrel is pulled through the fastener hole and causes a residual stress field around the hole. The plate is then loaded with a remote uniaxial stress of 40 ksi (276 MPa). The objective here is to compute K_I for a through-the-thickness crack length c/R = 0.8 (c = .104 inch = 2.65 mm).

In order to apply the superposition calculation to the coldworked hole configuration, it is again necessary to determine the hoop stress distribution for the uncracked case. One may, for example, establish the coldworked hole residual stress field by the "exact" elastic-plastic solution given by Hsu and Forman (27) for an infinite sheet containing a pressurized circular hole. Their plane stress result is based on the J_2 deformation theory and modified Ramberg-Osgood law. A small computer program was written here to assist in solving the fairly involved equations which represent the Hsu-Forman solution and used to obtain the residual stress distributions shown in Figure 8. (Note that there are several typographical errors in the equations given in Reference 27).

Figure 8 indicates that large compressive hoop stresses are left next to the hole edge by the pre-expansion and are balanced further away from the hole by a corresponding tensile field. Since large tensile stresses are concentrated at the edge of an unworked hole when the plate is loaded in uniaxial tension, the residual stress distribution reduces the peak tension next to the hole. An opposite effect, which could lead to more plastic flow, and to a change in the residual stress pattern, would occur if the plate were loaded in compression following coldworking.

For example, the residual hoop stress in Figure 8 was fit to within three percent by a polynomial as before, and gave the following result.

$$\sigma_H = \sum_{n=0}^{3} B_n (x/R)^n \qquad (12)$$

$$= -130.53 + 296.25(x/R) - 226.67(x/R)^2 + 72.936(x/R)^3$$

Here the polynomial coefficients B_n have units of ksi and x/R is restricted to the range $0 \leq x/R \leq 1.0$. Now, the unflawed hoop stress for the remotely loaded coldworked hole is found by adding Eqs. 11 and 12. Letting σ = 40 ksi in Eq. 11 (the remote tensile stress of interest) gives

$$\sigma_{total} = \sigma_{remote} + \sigma_{coldwork} \qquad (13)$$

$$= \sum_{n=0}^{3} (\sigma A_n + B_n)(x/R)^n = \sum_{n=0}^{3} C_n (x/R)^n$$

$$= -13.770 + 84.838(x/R) + 23.626(x/R)^2 - 34.704(x/R)^3$$

Note that the superposition of Eq. 13 implies that the remote stress field is applied elastically and does not alter the residual stresses introduced by coldworking. Since the sum of the remote and residual stresses never exceeds yield, this superposition is valid for the present example.

Now, the desired stress intensity factor for the 0.104 inch long through-crack (c/R = 0.8) can be computed by superposition as before. Table 1 and Eq. 13 provide the following information.

M_0 = .8610	C_0 = -13.770 ksi
M_1 = .4693	C_1 = 84.838 ksi
M_2 = .3030	C_2 = 23.626 ksi
M_3 = .2089	C_3 = -34.704 ksi

The summation of Eq. 5 gives

$$K_I = \sum K_n = \sqrt{\pi c} \sum M_n C_n$$

$= \sqrt{(\pi)(.1044)}$ {(.8610)(-13.770) + (.4693)(84.838) + (.3030)(23.626) + (.2089)(-34.704)} = 15.96 ksi - $in^{1/2}$ = K_I.

This result is plotted as the large "star" on Figure 9, and is compared with experimental measurements on coldworked hole specimens reproduced from Reference 4. The line labeled "Coldwork" was obtained by superposition calculations similar to that employed here except that a higher order polynomial fit was used to extend the x/R range in Eqs. 11-13. The "zero K" values indicated for small crack lengths actually resulted from calculations which gave negative stress intensity factors (note that Eq. 13 gives negative hoop stresses for small x/R). Since negative K's have no physical meaning, all negative results were set equal to zero in Fig. 9. The line labeled "Bowie" is for the unworked case (remote load only). The experimental data were obtained from fatigue crack growth rate measurements in precracked coldworked hole specimens (see Reference 4 for additional details). Note that the predicted stress intensity factors agree well with the experimental data, indicating the superposition procedure can give good predictions for the coldworking process. Similar results are given in Reference 4 for other remote load applications, and indicate that the stress intensity factor calculations can provide good estimates of the fatigue crack growth lives of coldworked holes.

EXAMPLE 3: CORNER-CRACKED HOLE, REMOTE TENSION

Consider a corner crack emanating from an open hole as in Example 1. Stress intensity factors for this flaw configuration were obtained directly by the finite element - alternating method and are reported in Table 5. The goal of this example is to demonstrate application of the crack face pressure results in Table 4 by employing them to independently calculate the remote load results (Table 5) through the superposition procedure. The specific objective is to compute $K_I/(\sigma\sqrt{\pi a})$ at $\phi = 90°$ for a crack which has an aspect ratio a/c = 1.5 and length a/t = 0.8.

The unflawed hoop stress distribution is again given by Eq. 11, and Table 4 provides the appropriate crack face stress intensity coefficients M_n.

$$M_0 = .4994 \qquad A_0 = 2.9190\,\sigma$$

$$M_1 = .0939 \qquad A_1 = -5.2853\,\sigma$$

$$M_2 = .0280 \qquad A_2 = 6.2574\,\sigma$$

$$M_3 = .0027 \qquad A_3 = -2.6910\,\sigma$$

Equation 5 now gives

$$K_I = \sigma\sqrt{\pi a}\ \{(.4994)(2.9190) + (.0939)(-5.2853) + (.0280)(6.2574) + (.0027)(-2.6910)\} = 1.1294\ \sigma\sqrt{\pi a}$$

The corresponding result obtained by an independent application of the finite element - alternating method as described in Reference 10 and reported in Table 5, is $K_I(\sigma\sqrt{\pi a}) = 1.1660$ (a 3.1 percent difference). This difference could be due to the error in fitting the exact hoop stress solution by Eq. 11 or, as discussed earlier, to through-the-thickness effects, or to approximations employed by polynomial fitting routines in the finite element - alternating method.

EXAMPLE 4: SURFACE-CRACKED HOLE, REMOTE TENSION

Consider another plate with an open hole loaded in remote tension. For this example, assume a surface crack occurs along the bore of the hole (see Figure 6), and compute the variation in stress intensity factor around the perimeter of a crack which has an aspect ratio $a/c = 1.11$ and length $2a/T = 0.8$. The unflawed hoop stress is again given by Eq. 11, and the stress intensity factors are now found in Table 7. At the crack perimeter location defined by $\phi = 90^\circ$ (where the crack intersects the bore of the hole), the M_n are

$$M_0 = 0.6836$$

$$M_1 = 0.1030$$

$$M_2 = 0.0270$$

$$M_3 = 0.0061$$

Computing the stress intensity factor by Eq. 5 gives

$$K_I = \sum K_n = \sqrt{\pi c} \sum_{n=0}^{3} A_n M_n$$

$$= \sigma\sqrt{\pi c} \{(2.9190)(0.6836) - (5.2853)(0.1030) + (6.2574)(0.0270) - (2.6910)(0.0061)\} = 1.6036\,\sigma\sqrt{\pi c}$$

Note that the result obtained directly by the finite element - alternating method reported in Table 8 for this case ($a/c = 1.11$, $2a/T = 0.8$, $\phi = 90^0$) is $K_I = 1.625\,\sigma\sqrt{\pi c}$. Similar calculations for $\phi = 0^0$, 30^0, and 60^0 yield respective values of 0.995, 1.113, and 1.401 for $K_I\,\sigma\sqrt{\pi c}$. These results also compare quite favorably with the independent calculations reported in Table 8.

For comparison purposes, the superposition procedure described in Examples 3 and 4 was used to recompute all corner-cracked and surfaced-cracked hole results reported in Tables 5 and 8. In this manner, it was possible to determine the accuracy achieved by the superposition method for surface and corner cracks. For the surface cracked holes, the Table 8 results (remote loading applied directly) agreed within 5.3 percent of all stress intensity factors found from the crack face pressure solutions. The largest discrepancy occured at $\phi = 90°$ for the smallest cracks ($2a/T = 0.2$) for all three flaw shapes ($a/c = 1.11$, 1.5, and 2.0). For the corner-cracked holes, the Table 5 results agree within 9 percent of the superposition calculations (see Example 3) for all cases. The largest difference again occurred for the smallest crack lengths ($2a/T = 0.2$) at the point where the crack intersects the bore of the hole ($\phi = 0$ in Figure 5). In general, most calculations were well within 5 percent agreement.

Thus, these "calibration" computations indicate that the superposition procedure provides an effective means for estimating the stress intensity

factor distribution around the perimeter of corner- and surface-cracked holes. The fact that the greatest "error" occurs for the smallest crack lengths along the bore of the hole is consistent with the thickness variation in hoop stress (20) described earlier.

EXAMPLE 5: CORNER-CRACKED COLDWORKED HOLES

For the final example, consider a corner crack which occurs at the coldworked hole described in Example 2. Assume the crack shape a/c = 1.1, the flaw length a/T = 0.4 (a = 0.104 in = 2.65 mm), and the remote applied stress is 45 ksi (310 MPa). The uncracked hoop stress can again be found by adding the remote and residual coldworked hole stresses as in Eq. 13 (in this case, σ = 45 ksi). For this example, the Eq. 13 calculation and Table 4 gives the following for ϕ = 0.

$$M_0 = 0.6656 \qquad C_0 = 0.8250 \text{ ksi}$$
$$M_1 = 0.3329 \qquad C_1 = 58.41 \text{ ksi}$$
$$M_2 = 0.1943 \qquad C_2 = 54.91 \text{ ksi}$$
$$M_3 = 0.1202 \qquad C_3 = -48.16 \text{ ksi}$$

The superposition calculation now gives

$$K_I = \sum_{n=0}^{3} K_n = \sqrt{\pi a} \sum_{n=0}^{3} M_n C_n = 14.22 \text{ Ksi-in}^{1/2}$$

Similar calculations at other points around the crack border (ϕ = 30°, 60°, and 90°) give K_I values of 12.69, 7.15, and 3.16 Ksi-in$^{1/2}$.

Note that for an identical crack in a plate which is not coldworked, but subjected to the remote tensile stress only, the results of Table 5 (or approximate calculations with the Table 4 crack face pressure solutions as in Example 5) give K_I values of 26.4, 26.0, 31.3 and 37.2 Ksi-in$^{1/2}$. for the respective parametric angles ϕ = 0°, 30°, 60°, and 90°. The large reduction in K_I for the coldworked hole case is consistent with the experimental

fact that coldworking can significantly reduce fatigue crack growth rates at fastener holes. Note that the reduction in K_I is greatest at the bore of the hole ($\phi = 90^0$) where coldworking lowers K_I to 3.16 Ksi-in$^{1/2}$ from 37.2 Ksi-in$^{1/2}$, indicating that coldworking is most effective next to the hole edge.

SECTION V

SUMMARY AND CONCLUSIONS

The objective of this report is to present a set of general stress intensity factor solutions which may be used to analyze practical fastener hole problems. Results are given for radial through-the-thickness, quarter-elliptical corner, and semielliptical surface (embedded) cracks which are loaded with crack face pressure. Through linear superposition, these tabulated results are readily applied to other types of loading. This superposition procedure is demonstrated through several sets of example calculations.

It is felt that the dimensionless stress intensity factors reported in Tables 1, 2, 4, and 7 provide an effective means for estimating K_I for practical fastener hole crack configurations. In applying these crack face pressure solutions to new problems, however, the designer or analyst should consider the following points.

1. The crack face pressure (unflawed crack plane hoop stresses) should be tension over the entire crack.
2. The unflawed hoop stresses must be adequately described by the polynomial expression given by Eq. 2. Through-the-thickness problems can employ a sixth degree fit, while the corner and surface crack geometries are limited to third order polynomials. Note, however, that it is only necessary to represent the hoop stress over the range $0 \leq X/R \leq c$.

3. Through-the-thickness variations in the crack face pressure are not considered. Thus, caution should be exercised in applying the crack face pressure solutions to situations where the unflawed hoop stress exhibits a significant through-the-thickness variation. The remote stress results reported in Tables 4 and 8 do, however, contain through-the-thickness effects.

4. The corner and surface crack results are restricted to plates which have hole diameters equal to the plate thickness (2R=T) and to materials with a Poisson's ratio of 0.25.

Questions will naturally arise regarding extrapolation of the present results to cases of differing hole diameters to plate thickness ratios, loading conditions and crack shapes or sizes. Kullgren and Smith (9, 10) list four effects governing the magnitude and variation of mode-one stress intensity along the crack border.

1. Hole Stress Concentrations. Locations on the crack border close to the hole and thus in a region of elevated stress have larger stress intensity factors than do locations more removed.
2. Front and Back Surfaces. Crack points close to a plate front or back surface or near a crack intersection with these surfaces have elevated stress intensity factors.
3. Hole Surface. For small cracks (relative to hole diameter) the hole surface has an effect similar to crack intersection with the plate front or back surfaces. For large cracks, the hole restricts crack opening resulting in lower stress intensity near the hole/crack intersection.
4. Crack Shape. Stress intensity factors are highest at the ends of an elliptical crack under constant load (9).

In general, it is not possible from the present results to separate or determine the relative importance of these effects. Any change to the crack or plate geometries results in more than one effect operating. For example, earlier work (7, 9, 10) indicates a reduction of 2R/T from 1.0 to 0.5 while all other parameters remain unchanged resulted in a lowering of magnification factors at all locations on the crack border for cases of remote loading (open fastener hole). However, when this same load is transferred to a fastener in the hole, magnification factors increased for the same reduction in 2R/T. While this surely underscores the importance of the Hole Stress Concentration Effect, it is by no means clear that for other plate/crack geometries the same trend will be seen. In the absence of an extension of the present work, the authors do not recommend the quantitative extrapolation of the results presented here.

REFERENCES

1. Coffin, M.D. and Tiffany, D.F., "New Air Force Requirements for Structural Safety, Durability, and Life Measurement", Journal of Aircraft, Vol. 13, No. 2, 1976, pp. 93-98.

2. Petrak, G.J. and Stewart, R.P., "Retardation of Cracks Emanating from Fastener Holes", Engineering Fracture Mechanics, Vol. 6, No. 2, 1974, pp. 275-282.

3. Phillips, J.L., "Sleeve Coldworking Fastener Holes", Technical Report AFML-TR-740-10, Air Force Materials Laboratory, Wright-Patterson Air Force Base, Ohio, February, 1974.

4. Cathey, W.H. and Grandt, A.F., Jr., "Fracture Mechanics Consideration of Residual Stresses and Introduced by Coldworking Fastener Holes", Journal of Engineering Materials and Technology, Vol. 102, No. 2, January 1980, pp. 85-91.

5. Grandt, A.F., Jr., "Stress Intensity Factors for Some Through-Cracked Fastener Holes", International Journal of Fracture, Vol. 11, No. 2, April 1975, pp. 283-294.

6. Bowie, O.L., "Analysis of an Infinite Plate Containing Radial Cracks Originating at the Boundary of an Internal Circular Hole", Journal of Mathematics and Physics, Vol. 35, 1956, pp. 60-71.

7. Kullgren, T.E., Smith, F.W., and Ganong, G.P., "Quarter-Elliptical Cracks Emanating from Holes in Plates", Journal of Engineering Materials and Technology, Vol. 100, April 1978, pp. 144-149.

8. Kullgren, T.E. and Smith, F.W., "The Finite Element-Alternating Method Applied to Benchmark No. 2", International Journal of Fracture, Vol. 14, 1978, pp. R319-R322.

9. Kullgren, T.E. and Smith, F.W., "Part-Elliptical Cracks Emanating from Open and Loaded Holes in Plates", Journal of Engineering Materials and Technology, Vol. 101, January 1979, pp. 12-17.

10. Smith, F.W. and Kullgren, T.E., "Theoretical and Experimental Analysis of Surface Cracks Emanating from Fastener Holes", Technical Report AFFDL-TR-76-104, Air Force Flight Dynamics Laboratory, Wright-Patterson Air Force Base, Ohio, 1977.

11. Wilson, E.L., "Finite Element Analysis of Mine Structure", Technical Report Bureau of Mines OF 27-73, Denver Mining Research Center, September 1972.

12. Shaw, R,C, and Kobayashi, A.S., "Stress Intensity Factors for an Elliptical Crack under Arbitrary Normal Loading", Engineering Fracture Mechanics, Vol. 3, No. 1, July 1971.

13. Tweed, J. and Rooke, D.P., "The Distribution of Stress Near the Tip of a Radial Crack at the Edge of a Circular Hole", International Journal of Engineering Science, Vol. 11, 1973, pp. 1185-1195.

14. Raju, I.S. and Newman, J.C., Jr., "Stress-Intensity Factors for Two Symmetric Corner Cracks", Fracture Mechanics, ASTM STP 677, 1979, pp. 411-430.

15. Kullgren, T.E. and Smith, F.W., "Static Fracture Testing of PMMA Plates Having Flawed Fastener Holes",Experimental Mechanics, Vol. 20, No. 3, March 1980, pp. 95-102.

16. Snow, J.R., "A Stress Intensity Factor Calibration for Corner Flaws at an Open Hole", Technical Report AFML-TR-74-282, Air Force Materials Laboratory, Wright-Patterson Air Force Base, Ohio, 1975

17. Petrak, G.J. and Ruschau, J.J., "Fatigue and Fatigue Crack Growth Characteristics of Improperly Quenched (Substrength) Aluminum", Engineering Fracture Mechanics, Vol 15, No. 1-2, 1981, pp 143-153.

18. Grandt, A.F., Jr., "Stress Intensity Factors for Cracked Holes and Rings Loaded with Polynomial Crack Face Pressure Distributions", International Journal of Fracture, Vol. 14, No. 4, August 1978, pp. R221-R229.

19. Grandt, A.F., Jr. and Kullgren, T.E., "Stress Intensity Factors for Corner Cracked Holes Under General Loading Conditions", Journal of Engineering Materials and Technology, Vol. 103, No. 2, April 1981, pp. 171-176.

20. Sternberg, E. and Sadowsky, M.S., "Three-Dimensional Solution for the Stress Concentration Around a Circular Hole in a Plate of Arbitrary Thickness ", Journal of Applied Mechanics, Vol. 16, No. 1, 1949, pp. 27-38

21. Hill, R.J., Reimann, W.H., and Ogg, J.B., "A Retirement-For-Cause Study of an Engine Turbine Disk", draft manuscript, 1978.

22. Private correspondence with A.W. Gunderson, Wright Aeronautical Laboratories, Wright-Patterson Air Force Base, Ohio.

23. Hsu, T.M., McGee, W.M., and Aberson, J.A., "Extended Study of Flaw Growth at Fastener Holes", Technical Report AFFDL-TR-77-83, Air Force Flight Dynamics Laboratory, Wright-Patterson Air Force Base, Ohio, 1977.

24. Grandt, A.F., Jr., "Crack Face Pressure Loading of Semielliptical Cracks Located Along the Bore of a Hole", Engineering Fracture Mechanics Vol. 14, No. 4, 1981, pp. 843-852.

25. Paris, P.C. and Sih, G.C., "Stress Analysis of Cracks", Fracture Toughness Testing and its Applications, ASTM STP 381, 1964, pp. 30-81.

26. Timoshenko, S. and Goodier, J.N., Theory of Elasticity, 2nd ed., McGraw-Hill Book Company, New York, P. 80.

27. Hsu, Y.C. and Forman, R.G., "Elastic-Plastic Analysis of an Infinite Sheet Having a Circular Hole Under Pressure", ASME Journal of Applied Mechanics, Vol. 42, No. 2, 1975, pp. 347-352.

Table 1. Dimensionless stress intensity factors for a single-cracked hole loaded with a crack face pressure $p(x) = A_n(x/R)^n$.

$\frac{c}{R}$	$K_n/(A_n\sqrt{\pi c})$						
	n						
	0	1	2	3	4	5	6
.10	.9934E+00	.6348E-01	.4994E-02	.4244E-03	.3756E-04	.3405E-05	.3137E-06
.20	.9817E+00	.1255E+00	.1980E-01	.3369E-02	.5968E-03	.1083E-03	.1996E-04
.30	.9592E+00	.1859E+00	.4415E-01	.1130E-01	.3004E-02	.8181E-03	.2263E-03
.40	.9351E+00	.2447E+00	.7785E-01	.2661E-01	.9449E-02	.3434E-02	.1267E-02
.50	.9119E+00	.3020E+00	.1207E+00	.5167E-01	.2297E-01	.1044E-01	.4820E-02
.60	.8914E+00	.3583E+00	.1725E+00	.8882E-01	.4744E-01	.2590E-01	.1436E-01
.80	.8610E+00	.4693E+00	.3030E+00	.2089E+00	.1490E+00	.1086E+00	.8036E-01
1.00	.8442E+00	.5805E+00	.4702E+00	.4060E+00	.3625E+00	.3306E+00	.3059E+00
1.25	.8361E+00	.7214E+00	.7319E+00	.7907E+00	.8833E+00	.1008E+01	.1166E+01
1.50	.8337E+00	.8639E+00	.1052E+01	.1365E+01	.1831E+01	.2506E+01	.3480E+01
1.75	.8308E+00	.1006E+01	.1431E+01	.2167E+01	.3391E+01	.5418E+01	.8778E+01
2.00	.8248E+00	.1147E+01	.1865E+01	.3232E+01	.5783E+01	.1056E+02	.1956E+02
2.50	.8037E+00	.1418E+01	.2900E+01	.6292E+01	.1409E+02	.3220E+02	.7458E+02

Table 2. Dimensionless stress intensity factors for a double-cracked hole loaded with a crack face pressure $p(x) = A_n (x/R)^n$.

$\frac{c}{R}$	$K_n/(A_n\sqrt{\pi c})$						
	n						
	0	1	2	3	4	5	6
.10	.1001E+01	.6433E-01	.5062E-02	.4295E-03	.3795E-04	.3435E-05	.3161E-06
.20	.9752E+00	.1257E+00	.1985E-01	.3380E-02	.5986E-03	.1086E-03	.2001E-04
.30	.9651E+00	.1870E+00	.4439E-01	.1135E-01	.3017E-02	.8211E-03	.2271E-03
.40	.9582E+00	.2484E+00	.7869E-01	.2683E-01	.9515E-02	.3454E-02	.1274E-02
.50	.9529E+00	.3097E+00	.1228E+00	.5235E-01	.2321E-01	.1054E-01	.4857E-02
.60	.9485E+00	.3711E+00	.1767E+00	.9043E-01	.4812E-01	.2621E-01	.1450E-01
.80	.9434E+00	.4949E+00	.3143E+00	.2145E+00	.1522E+00	.1105E+00	.8154E-01
1.00	.9542E+00	.6210E+00	.4924E+00	.4199E+00	.3723E+00	.3379E+00	.3115E+00
1.25	.9670E+00	.7822E+00	.7735E+00	.8235E+00	.9119E+00	.1034E+01	.1191E+01
1.50	.9816E+00	.9467E+00	.1121E+01	.1429E+01	.1898E+01	.2581E+01	.3566E+01
1.75	.9943E+00	.1113E+01	.1533E+01	.2279E+01	.3528E+01	.5594E+01	.9015E+01
2.00	.1015E+01	.1260E+01	.2012E+01	.3415E+01	.6037E+01	.1093E+02	.2013E+02
2.50	.1027E+01	.1[illegible]E+01	[illegible]E+01	.6712E+01	.1481E+02	.3351E+02	.7708E+02

Table 3 Summary of Corner-Cracked Hole Solutions

(x denotes geometries analyzed)

Crack Shape a/c	Crack Size a/T	Loading				
		Crack face pressure $A_n(x/R)^n$				Remote Uniaxial Tension
		n=0	n=1	n=2	n=3	σ
.5	.2	x	x	x	x	x
	.4	x	x	x	x	x
	.5	x	x	x	x	x
.9	.2	x	x	x	x	x
	.4					
	.6					
	.8	x	x	x	x	x
1.1	.2	x	x	x	x	x
	.4	x	x	x	x	x
	.6	x	x	x	x	x
	.8	x	x	x	x	x
	1.0	x	x	x	x	x
1.5	.2	x	x	x	x	x
	.4	x	x	x	x	x
	.6	x	x	x	x	x
	.8	x	x	x	x	x
	1.0	x	x	x	x	

Table 4 Stress Intensity Magnification Factors ($M_n = K_n/A_n\sqrt{\pi a}$) for Corner-Cracked Holes Loaded With Crack Face Pressure $A_n(x/R)^n$

a/c=0.5

	ϕ Parametric Angle From Front Surface		0°	30°	60°	90°
		n=0	.6737	.7704	.8448	.7877
		1	.4228	.4383	.2818	.0968
a/t=0.2	M_n	2	.2867	.2636	.1198	.0237
		3	.2000	.1700	.0592	.0068
		n=0	.7702	.8066	.8459	.8069
		1	.9193	.9015	.5624	.2152
a/t=0.4	M_n	2	1.2176	1.0806	.4804	.1106
		3	1.6790	1.3912	.4772	.0667
		n=0	.8055	.8295	.8610	.8137
		1	1.1751	1.1359	.7095	.2812
a/t=0.5	M_n	2	1.9292	1.6916	.7535	.1880
		3	3.3114	2.7133	.9309	.1507

a/c=0.9

	ϕ Parametric Angle From Front Surface		0°	30°	60°	90°
		n=0	.6475	.6865	.6874	.6377
		1	.2056	.1989	.1196	.0444
a/t=0.2	M_n	2	.0745	.0642	.0273	.0049
		3	.0283	.0224	.0070	.0002
		n=0	.8307	.7346	.6682	.6525
		1	.9880	.8339	.4634	.2142
a/t=0.8	M_n	2	1.3871	1.0761	.4240	.1175
		3	2.0761	1.5074	.4382	.0552

Table 4 (Cont'd) Stress Intensity Magnification Factors ($M_n = K_n/A_n\sqrt{\pi a}$) for Corner-Cracked Holes Loaded with Crack Face Pressure $A_n(x/R)^n$

a/c=1.1

		φ Parametric Angle From Front Surface	0°	30°	60°	90°
		n=0	.6725	.6851	.6418	.5855
		1	.1684	.1575	.0893	.0335
a/t=0.2	M_n	2	.0490	.0411	.0165	.0030
		3	.0152	.0117	.0034	.0000
		n=0	.6656	.6369	.6044	.5852
		1	.3329	.2975	.1682	.0736
a/t=0.4	M_n	2	.1943	.1572	.0622	.0149
		3	.1202	.0900	.0256	.0016
		n=0	.7488	.6698	.6006	.5791
		1	.5511	.4638	.2511	.1158
a/t=0.6	M_n	2	.4773	.3669	.1395	.0387
		3	.4403	.3149	.0863	.0101
		n=0	.7732	.6784	.6065	.5921
		1	.7464	.6213	.3357	.1588
a/t=0.8	M_n	2	.8555	.6531	.2475	.0698
		3	1.0479	.7459	.2029	.0223
		n=0	.8832	.7389	.7912	.9374
		1	1.0779	.8694	.4756	.2675
a/t=1.0	M_n	2	1.5434	1.1484	.3989	.0894
		3	2.3617	1.6443	.3605	.0000

a/c=1.5

		φ Parametric Angle From Front Surface	0°	30°	60°	90°
		n=0	.6296	.6378	.5678	.5031
		1	.1126	.1033	.0547	.0204
a/t=0.2	M_n	2	.0239	.0196	.0072	.0013
		3	.0054	.0041	.0010	.0000
		n=0	.6304	.5976	.5365	.4997
		1	.2262	.1983	.1045	.0444
a/t=0.4	M_n	2	.0960	.0760	.0277	.0062
		3	.0435	.0317	.0079	.0001
		n=0	.6812	.6042	.5203	.4917
		1	.3632	.2998	.1516	.0689
a/t=0.6	M_n	2	.2300	.1730	.0601	.0157
		3	.1557	.1085	.0256	.0014
		n=0	.6976	.6103	.5246	.4994
		1	.4893	.4011	.2027	.0939
a/t=0.8	M_n	2	.4103	.3076	.1069	.0280
		3	.3689	.2567	.0606	.0027
		n=0	1.0755	.9059	.9488	1.0814
		1	.9536	.7549	.3949	.2240
a/t=1.0	M_n	2	1.0242	.7256	.2344	.0544
		3	1.1235	.7580	.1410	.0000

Table 5 Stress Intensity Magnification Factors for Corner Crack Holes Loaded with a Remote Uniaxial Stress σ

a/c	a/t	$M=K_I/(\sigma\sqrt{\pi a})$			
		$\phi=0$	30^o	60^o	90^o
.5	.2	.930	1.064	1.514	1.890
	.4	.954	.931	1.269	1.762
	.5	.982	.929	1.217	1.696
.9	.2	1.106	1.220	1.482	1.640
	.4	1.050	.999	1.235	1.543
	.6	1.060	.944	1.114	1.421
	.8	1.068	.906	1.041	1.369
1.1	.2	1.235	1.312	1.456	1.539
	.4	1.027	1.009	1.215	1.447
	.6	1.059	.952	1.090	1.338
	.8	1.038	.896	1.019	1.292
	1.0	1.121	.899	1.311	1.947
1.5	.2	1.263	1.347	1.383	1.365
	.4	1.070	1.069	1.190	1.302
	.6	1.050	.969	1.059	1.210
	.8	1.009	.903	.991	1.166
	1.0	1.465	1.242	1.750	2.386

Table 6 Summary of Semielliptical Surface Crack Hole Solutions (x denotes problem analyzed, 2R = T in all cases)

Crack Shape a/c	Crack Size 2a/T	Loading				
		Crack face pressure $A_n(x/R)^n$				Remote Uniaxial Tension
		n=0	n=1	n=2	n=3	σ
1.11	0.2	x	x	x	x	x
	0.4	x	x	x	x	x
	0.6	x	x	x	x	x
	0.8	x	x	x	x	x
	1.0	x	x	x	x	x
1.50	0.2	x	x	x	x	x
	0.4	x	x	x	x	x
	0.6	x	x	x	x	x
	0.8	x	x	x	x	x
	1.0	x	x	x	x	x
2.0	0.2	x	x	x	x	x
	0.4	x	x	x	x	x
	0.6	x	x	x	x	x
	0.8	x	x	x	x	x
	1.0	x	x	x	x	x

Table 7 Stress Intensity Magnification Factors for Semielliptical Surface Cracks at Holes in a Plate Loaded with Crack Face Pressure $A_n(x/R)^n$ (2R = T for all cases).

a/c	2a/T	n	$M_n = K_n/(A_n\sqrt{\pi c})$			
			$\phi = 0°$	$\pm 30°$	$\pm 60°$	$\pm 90°$
1.11	0.2	0	.6761	.6800	.6674	.5973
		1	.0882	.0746	.0448	.0187
		2	.0129	.0098	.0042	.0011
		3	.0020	.0014	.0004	.0001
	0.4	0	.6336	.6526	.6697	.6189
		1	.1718	.1467	.0914	.0427
		2	.0507	.0386	.0168	.0053
		3	.0156	.0111	.0035	.0005
	0.6	0	.6276	.6465	.6710	.6361
		1	.2561	.2186	.1375	.0682
		2	.1139	.0868	.0381	.0128
		3	.0528	.0375	.0118	.0019
	0.8	0	.6453	.6650	.7003	.6836
		1	.3456	.2957	.1904	.1030
		2	.2040	.1560	.0706	.0270
		3	.1260	.0898	.0293	.0061
	1.0	0	.6565	.7250	.8943	1.0039
		1	.4379	.3863	.2840	.2022
		2	.3222	.2511	.1278	.0690
		3	.2484	.1791	.0640	.0215

Table 7 (Continued)

a/c	2a/T	n	$M_n = K_n/(A_n\sqrt{\pi c})$			
			$\phi = 0°$	$\pm 30°$	$\pm 60°$	$\pm 90°$
1.5	0.2	0	.7683	.7496	.6793	.5763
		1	.0705	.0582	.0325	.0130
		2	.0075	.0056	.0022	.0006
		3	.0009	.0006	.0002	.0000
	0.4	0	.7437	.7403	.6964	.6058
		1	.1406	.1172	.0683	.0307
		2	.0300	.0224	.0092	.0028
		3	.0068	.0047	.0013	.0002
	0.6	0	.7110	.7185	.6982	.6256
		1	.2056	.1723	.1030	.0497
		2	.0667	.0498	.0207	.0068
		3	.0228	.0157	.0045	.0006
	0.8	0	.7159	.7248	.7157	.6607
		1	.2748	.2307	.1406	.0734
		2	.1189	.0889	.0378	.0139
		3	.0543	.0376	.0110	.0018
	1.0	0	.7270	.7831	.8820	.9088
		1	.3465	.2992	.2047	.1349
		2	.1872	.1423	.0670	.0332
		3	.1067	.0744	.0235	.0064

Table 7 (Continued)

a/c	2a/T	n	$M_n = K_n/(A_n\sqrt{\pi c})$			
			$\phi = 0°$	$\pm 30°$	$\pm 60°$	$\pm 90°$
2.0	0.2	0	.8345	.8008	.6833	.5406
		1	.0553	.0448	.0234	.0086
		2	.0044	.0032	.0012	.0003
		3	.0004	.0003	.0001	.0000
	0.4	0	.8393	.8152	.7114	.5718
		1	.1137	.0929	.0503	.0205
		2	.0179	.0131	.0050	.0013
		3	.0030	.0020	.0005	.0000
	0.6	0	.8024	.7952	.7212	.5959
		1	.1661	.1372	.0771	.0342
		2	.0397	.0292	.0114	.0034
		3	.0101	.0068	.0017	.0001
	0.8	0	.7847	.7877	.7359	.6262
		1	.2184	.1815	.1050	.0505
		2	.0700	.0517	.0207	.0069
		3	.0239	.0162	.0042	.0004
	1.0	0	.7831	.8297	.8651	.8052
		1	.2739	.2327	.1477	.0866
		2	.1099	.0821	.0357	.0154
		3	.0469	.0319	.0088	.0016

Table 8 Stress Intensity Magnification Factors for Semielliptical Surface Cracks at Holes in Large Plates Loaded with Uniaxial Tensile Stress σ (2R = T in all cases).

a/c	2a/T	$M = K_I/(\sigma\sqrt{\pi c})$			
		$\phi = 0°$	$\pm 30°$	$\pm 60°$	$\pm 90°$
1.11	0.2	1.608	1.687	1.803	1.733
	0.4	1.244	1.375	1.619	1.681
	0.6	1.081	1.204	1.474	1.620
	0.8	1.021	1.132	1.413	1.625
	1.0	0.971	1.166	1.710	2.206
1.50	0.2	1.956	1.970	1.904	1.702
	0.4	1.630	1.711	1.786	1.696
	0.6	1.382	1.491	1.650	1.654
	0.8	1.275	1.378	1.564	1.640
	1.0	1.211	1.403	1.817	2.095
2.0	0.2	2.227	2.192	1.968	1.620
	0.4	1.994	2.019	1.913	1.644
	0.6	1.725	1.801	1.810	1.632
	0.8	1.554	1.648	1.723	1.619
	1.0	1.445	1.629	1.904	1.944

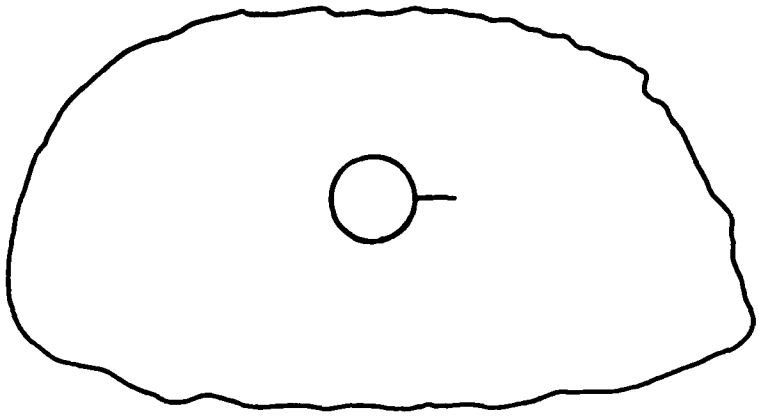

Through-The-Thickness Crack

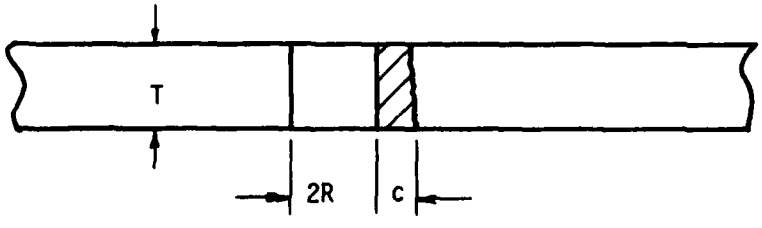

Quarter-Elliptical Corner Crack

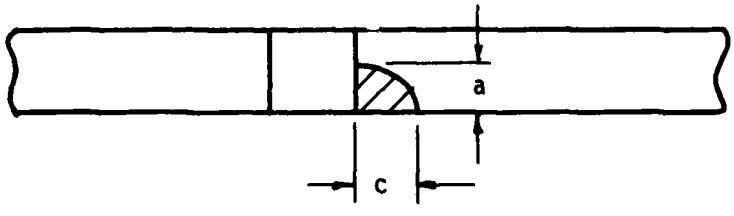

Semielliptical Surface Crack

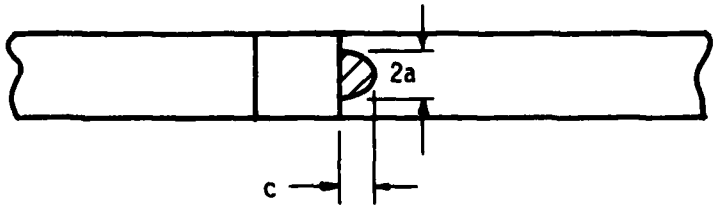

Figure 1 Flawed Fastener Hole Configurations

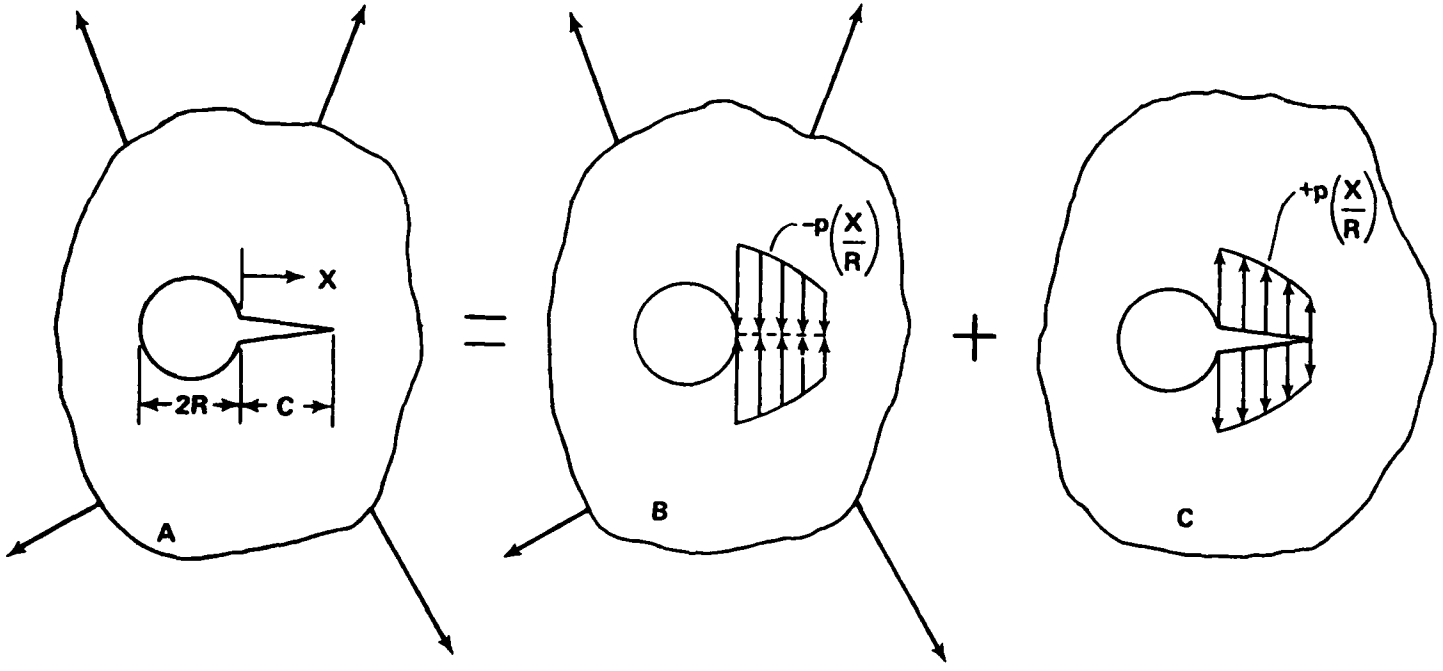

Figure 2: Schematic of linear superposition showing equivalence between remote load and crack face pressure stress intensity factor

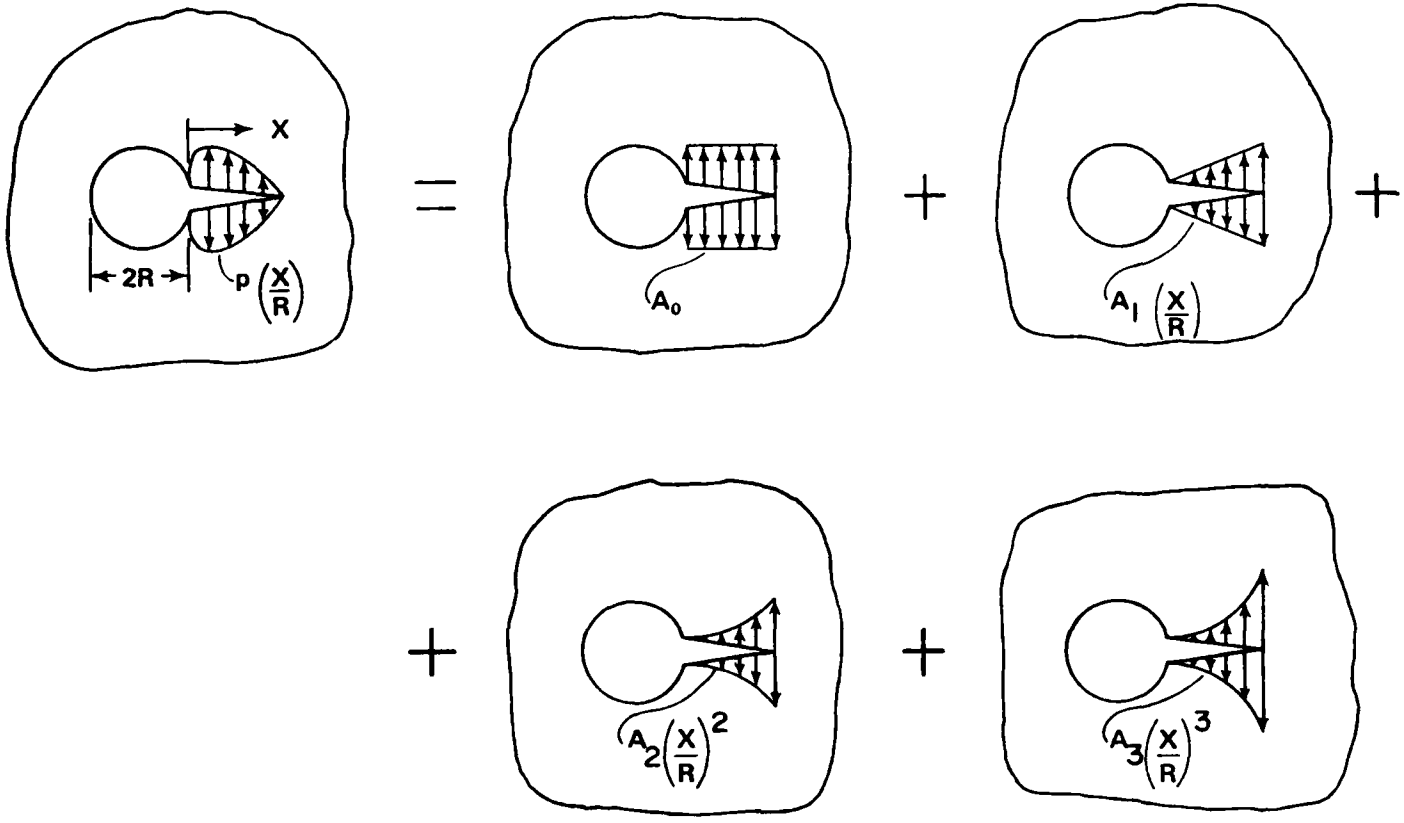

Figure 3: Schematic of crack face pressure problem resolved into components represented by a polynomial expansion for p(X/R)

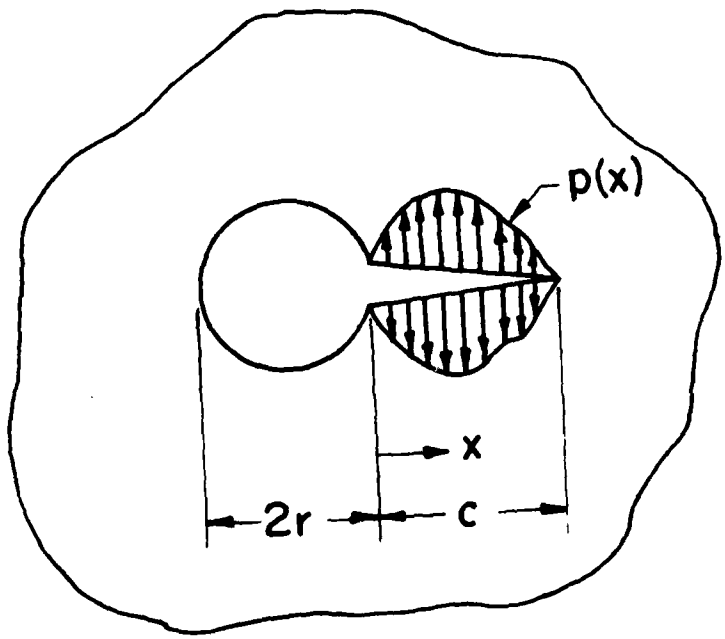

Figure 4: Crack face pressure loading p(x) applied to a radial through-the-thickness crack in an infinite sheet.

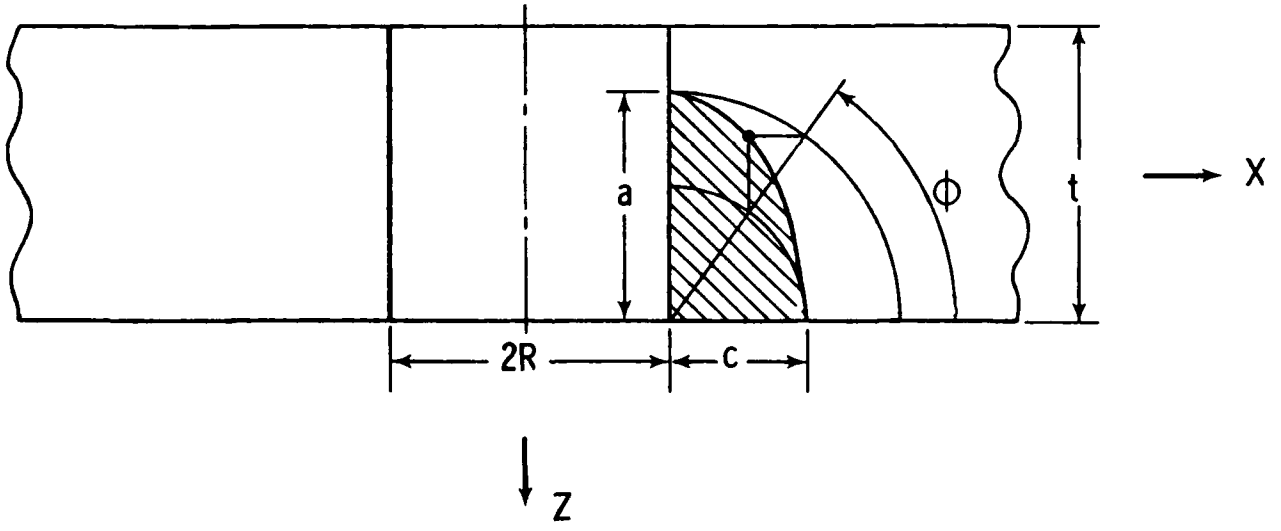

Figure 5: Quarter-elliptical corner crack located perpendicular to edge of hole in a wide plate.

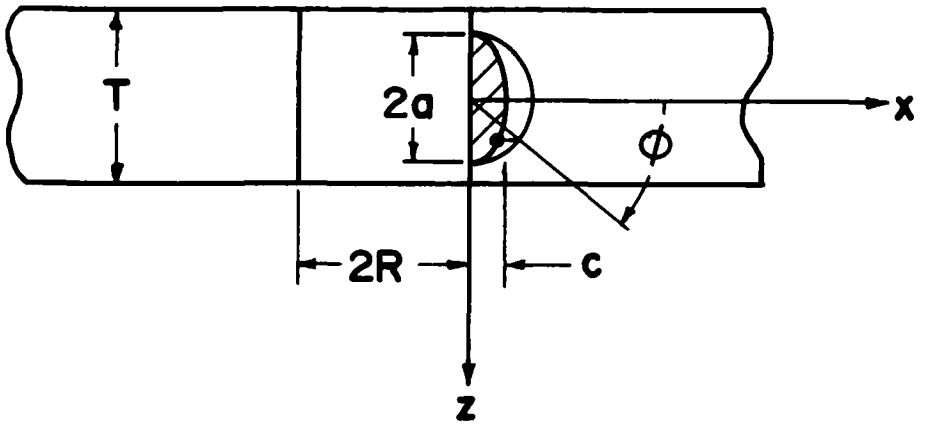

Figure 6: Semielliptical surface (embedded) crack located along bore of a hole in a large plate.

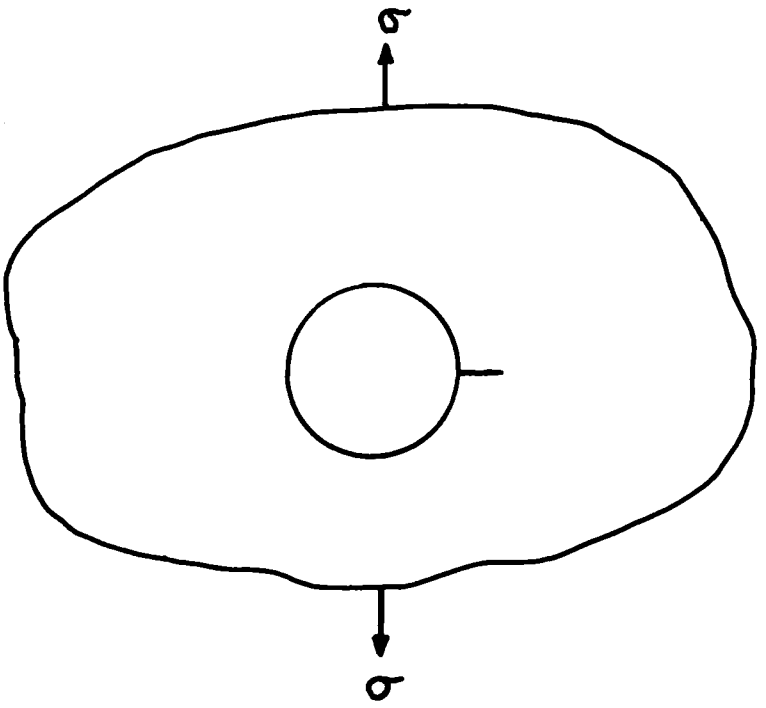

Figure 7: Cracked hole in a large plate loaded with remote tensile stress applied perpendicular to the crack plane

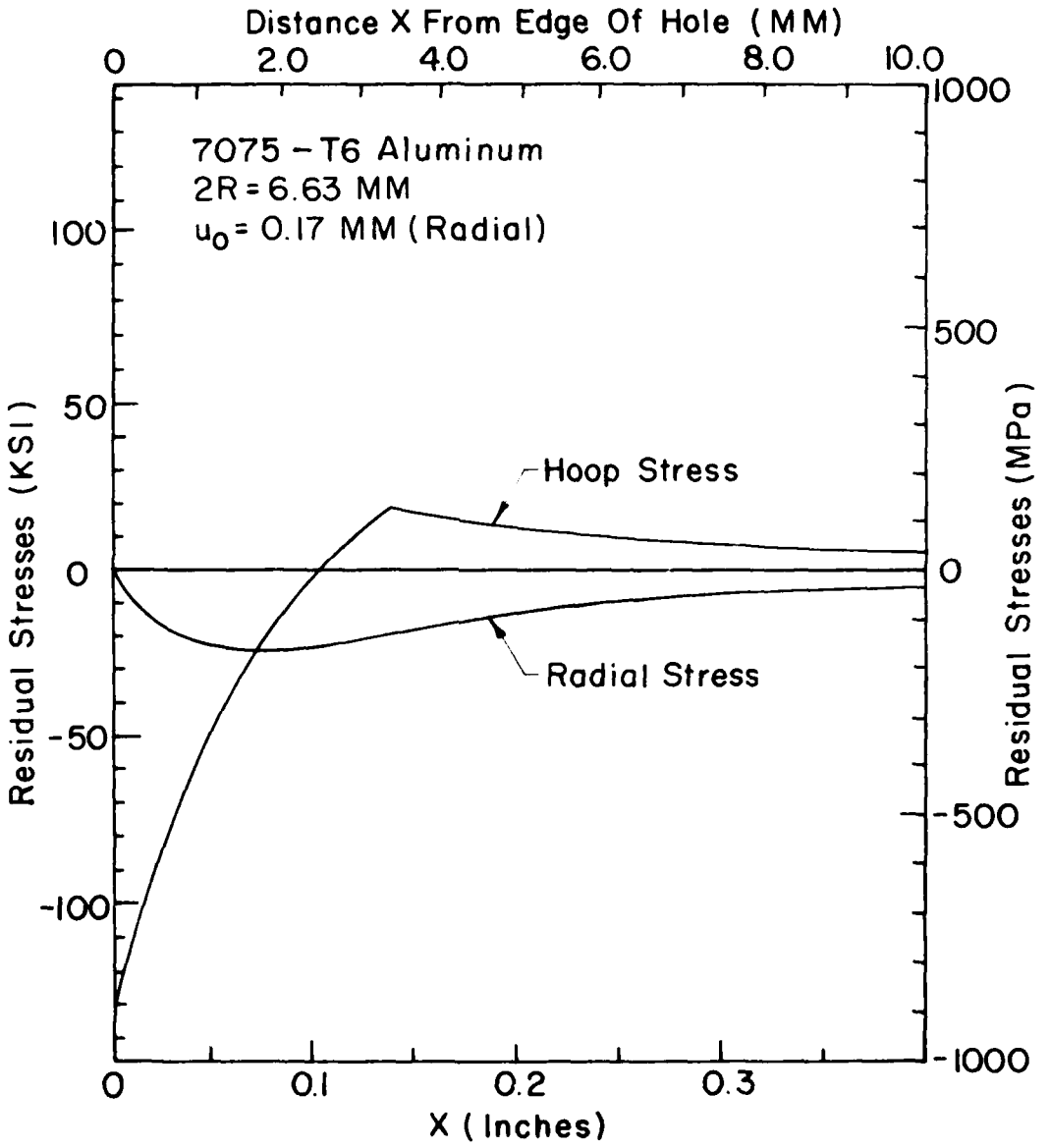

Figure 8: Residual stress distribution due to coldworking hole as predicted by Hsu-Forman solution

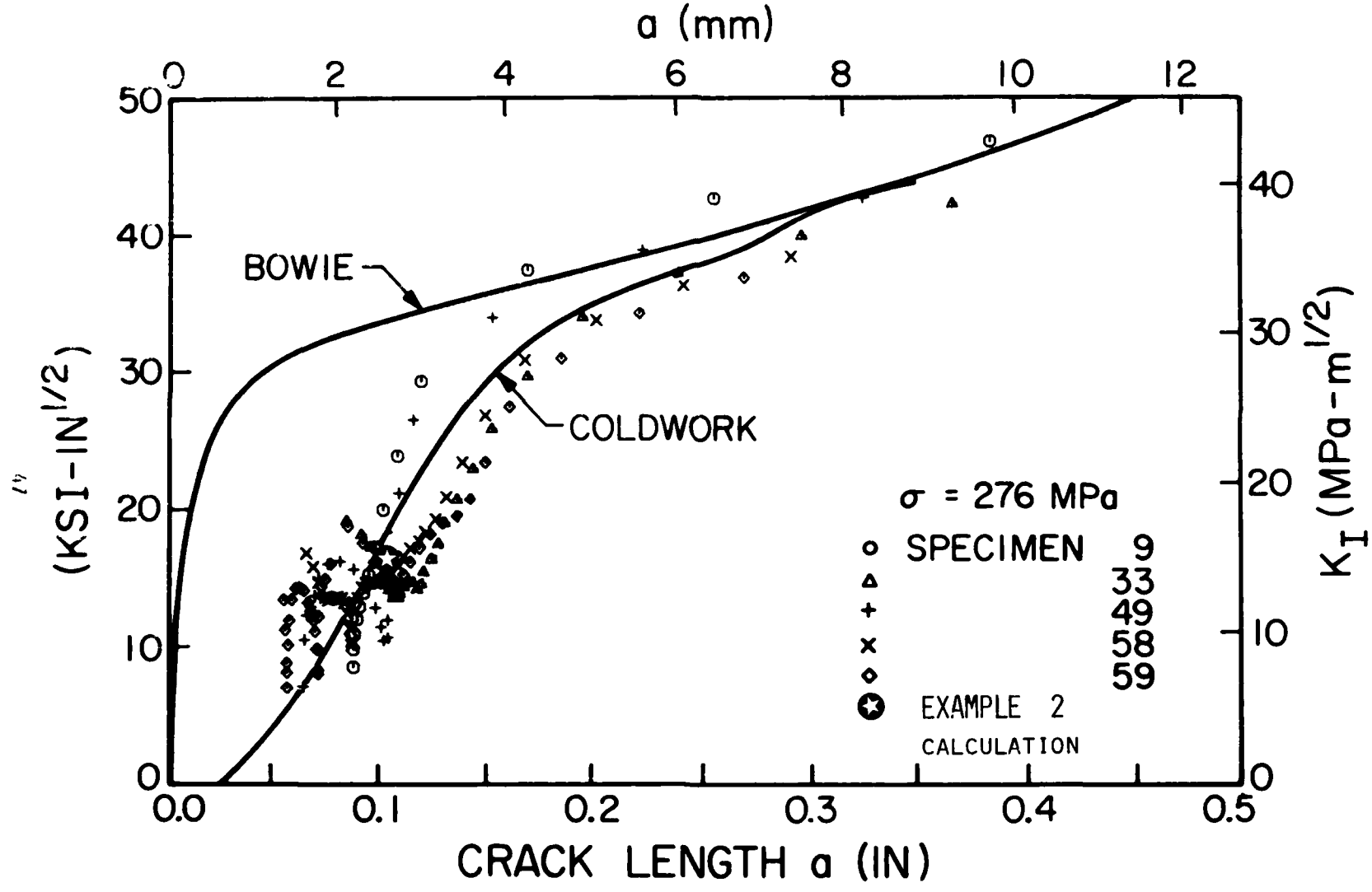

Figure 9: Comparison of predicted and experimental stress intensity factor calibration for coldworked hole specimens, 276 MPa(40 ksi) load

APPENDIX A

TABULAR DATA

1. INTRODUCTION

Appendices A through C are designed to provide completeness to this report. In Appendix A, results from finite element-alternating method calculations are listed for all 150 cases considered. Appendix B describes two short computer programs which can be used to regenerate more comprehensive descriptions of mode one stress intensity variations along the crack border. Appendix C contains another short program which gives crack opening displacements. The computer programs of Appendices B and C use the tabular results of Appendix A as input.

2. DATA DESCRIPTION

Table A-1 lists important geometric and loading parameters for the 75 surface crack cases and Table A-2 lists similar information for the 85 corner crack cases. Table A-3 lists 10 coefficients for each individual case. These coefficients result from the original finite element-alternating method calculations and must be used as input data for the computer programs described in Appendices B and C. A list of coefficients for cases different than those considered in the present report is contained in Reference 10. These coefficients can also be used in the computer programs of the following Appendices.

The actual plate modeled by the finite element - alternating method had a thickness of 1.0 and a radius 0.5. The objective was to compute stress intensity factors for crack pressures $p(x/R) = A_n(x/R)^n = \frac{A_n}{R^n} x^n$. Since R = .5, the actual loadings considered for the current model were $p(x) = (A_n/R^n)x^n = 1, 2x, 4x^2, 8x^3$ for n = 0, 1, 2, 3. In a few cases denoted in Table A-2, the pressure was $p(x) = 1, x, x^2, x^3$. These results were converted to the standard loading by multiplication by an appropriate constant. Thus, all of the results given in Tables 4 and 7 are for $p(x/R) = 1, (x/R), (x/R)^2, (x/R)^3$ which is equivalent to $p(x) = 1, 2x, 4x^2, 8x^3$ for the actual model (R = 0.5).

Table A-1. Surface Crack Cases

Case Number	Crack Type	a/c	2a/t	Loading Case, p(x) =				
				Remote Tension	1	2x	$4x^2$	$8x^3$
100	Surface	2.0	.2	x				
101					x			
102						x		
103							x	
104								x
105			.4	x				
106					x			
107						x		
108							x	
109								x
110			.6	x				
111					x			
112						x		
113							x	
114								x
115			.8	x				
116					x			
117						x		
118							x	
119								x
120			1.0	x				
121					x			
122						x		
123							x	
124								x

Table A-1. (cont'd)

Case Number	Crack Type	a/c	2a/t	Loading Case, p(x) = Remote Tension	1	2x	$4x^2$	$8x^3$
125	Surface	1.11	.2	x				
126					x			
127						x		
128							x	
129								x
130			.4	x				
131					x			
132						x		
133							x	
134								x
135			.6	x				
136					x			
137						x		
138							x	
139								x
140			.8	x				
141					x			
142						x		
143							x	
144								x
145			1.0	x				
146					x			
147						x		
148							x	
149								x

Table A-1. (cont'd)

Case Number	Crack Type	a/c	2a/t	Loading Case, p(x) = Remote Tension	1	2x	$4x^2$	$8x^3$
150	Surface	1.5	.2	x				
151					x			
152						x		
153							x	
154								x
155			.4	x				
156					x			
157						x		
158							x	
159								x
160			.6	x				
161					x			
162						x		
163							x	
164								x
165			.8	x				
166					x			
167						x		
168							x	
169								x
170			1.0	x				
171					x			
172						x		
173							x	
174								x

Table A-2. Corner Crack Cases

Case Number	Crack Type	a/c	a/t	Loading Case, p(x) = Remote Tension	1	2x	$4x^2$	$8x^3$
175	Corner	.5	.2	x				
176					x			
177						x		
178							x	
179								x
180			.4	x				
181					x			
182						x		
183							x	
184								x
185			.5	x				
186					x			
187						x*		
188							x*	
189								x*
190		.9	.2	x				
191					x			
192						x		
193							x	
194								x
195			.3	x				
196			.4	x				
197			.5	x				
198			.6	x				
199			.7	x				

* p(x) for these cases was x, x^2 and x^3

Table A-2. (cont'd)

Case Number	Crack Type	a/c	a/t	Loading Case, p(x) = Remote Tension	1	2x	$4x^2$	$8x^3$
200	Corner		.8	x				
201					x			
202						x		
203							x	
204								x
205			.9	x				
206		1.1	.1	x				
207			.2	x				
208					x			
209						x*		
210							x*	
211								x*
212			.3	x				
213			.4	x				
214					x			
215						x		
216							x	
217								x
218			.5	x				
219			.6	x				
220					x			
221						x		
222							x	
223								x

* p(x) for these cases was x, x^2 and x^3

Table A-2. (cont'd)

Case Number	Crack Type	a/c	a/t	Loading Case, p(x) = Remote Tension	1	2x	$4x^2$	$8x^3$
224	Corner		.7	x				
225			.8	x				
226					x			
227						x		
228							x	
229								x
230			.9	x				
231		1.5	.2	x				
232					x			
233						x		
234							x	
235								x
236			.4	x				
237					x			
238						x		
239							x	
240								x
241			.6	x				
242					x			
243						x		
244							x	
245								x
246			.8	x				
247					x			
248						x		
249							x	
250								x

Table A-2. (cont'd)

Case Number	Crack Type	a/c	a/t	Loading Case, p(x) =				
				Remote Tension	1	2x	$4x^2$	$8x^3$
251	Corner	1.5	1.0	x				
252					x			
253						x		
254							x	
255								x
256	Corner	1.1	1.0	x				
257					x			
258						x		
259							x	
260								x

Table A-3. Coefficients from Finite Element-Alternating Method Results

CASE	C00	C10	C01	C20	C11	C02	C30	C21	C12	C03
100	.5482E-11	0.	.7962E-13	-.211E-14	0.	.8141E-15	0.	.6244E-17	0.	-.7749E-18
101	.1884E-11	0.	.3234E-13	-.2679E-15	0.	.2268E-15	0.	.3222E-17	0.	-.1649E-18
102	.4659E-13	0.	.3183E-14	.4273E-16	0.	-.1970E-16	0.	.1733E-18	0.	-.9388E-20
103	.2624E-14	0.	.1965E-15	.4196E-17	0.	-.2181E-17	0.	.2061E-18	0.	-.4542E-19
104	.1662E-15	0.	.1354E-16	.4101E-18	0.	-.2117E-18	0.	.2996E-19	0.	-.6320E-20
105	.4408E-16	0.	.9577E-12	-.4366E-13	0.	.5173E-13	0.	.1317E-15	0.	-.1447E-15
106	.1643E-16	0.	.4853E-17	-.8145E-14	0.	.8755E-14	0.	-.1627E-16	0.	-.1936E-16
107	.9264E-12	0.	.9953E-13	.3220E-14	0.	-.1088E-14	0.	.1236E-16	0.	-.3097E-17
108	.9779E-13	0.	.1236E-13	.5873E-15	0.	-.2627E-15	0.	.5172E-16	0.	-.1182E-16
109	.1191E-13	0.	.1703E-14	.1109E-15	0.	-.5255E-16	0.	.1521E-16	0.	-.5257E-17
110	.1421E-05	0.	.3353E-11	-.4542E-12	0.	.2636E-12	0.	.4737E-14	0.	-.3412E-14
111	.5440E-14	0.	.2204E-11	-.1092E-12	0.	.7479E-13	0.	-.1890E-14	0.	-.5225E-15
112	.4645E-11	0.	.7153E-12	.3258E-13	0.	-.1133E-13	0.	-.2214E-15	0.	-.1056E-15
113	.7592E-12	0.	.1343E-12	.9572E-14	0.	-.4312E-14	0.	.1253E-14	0.	-.3133E-15
114	.1366E-12	0.	.2813E-13	.2816E-14	0.	-.1327E-14	0.	.5736E-15	0.	-.1262E-15
115	.3225E-09	0.	.7073E-11	-.2362E-11	0.	.1147E-11	0.	.1014E-12	0.	-.3145E-13
116	.1296E-09	0.	.6403E-11	-.7216E-12	0.	.3182E-12	0.	.4435E-14	0.	-.6837E-14
117	.1553E-10	0.	.2873E-11	.1447E-12	0.	-.5742E-13	0.	.3917E-15	0.	-.1485E-14
118	.3231E-11	0.	.7333E-12	.6437E-13	0.	-.3160E-13	0.	.1283E-13	0.	-.3223E-14
119	.7701E-12	0.	.2073E-12	.2665E-13	0.	-.1316E-13	0.	.7617E-14	0.	-.1733E-14
120	.6457E-09	0.	.1043E-10	-.1553E-10	0.	.4167E-11	0.	.1286E-11	0.	-.1559E-12

Table A-3. (cont'd)

CASE	C00	C10	C04	C20	C11	C02	C30	C21	C12	C03
121	.2721E-05	0.	.1434E-10	-.6164E-11	0.	.1359E-11	0.	.3446E-12	0.	-.4869E-13
122	.4065E-10	0.	.8494E-11	.5037E-13	0.	-.1775E-12	0.	.4863E-13	0.	-.1240E-13
123	.1643E-10	0.	.2744E-11	.2096E-12	0.	-.1430E-12	0.	.8621E-13	0.	-.2034E-13
124	.3041E-11	0.	.9857E-12	.1442E-12	0.	-.7752E-13	0.	.5861E-13	0.	-.1290E-13
125	.1412E-10	0.	.3477E-12	-.3226E-14	0.	.9327E-14	0.	.4991E-14	0.	-.3524E-16
126	.4661E-10	0.	.1684E-12	-.6832E-15	0.	.2490E-14	0.	.1432E-14	0.	-.4310E-17
127	.2374E-12	0.	.3010E-13	.1766E-15	0.	-.3429E-15	0.	.1227E-17	0.	-.4811E-18
128	.2312E-13	0.	.3320E-14	.3225E-16	0.	-.6760E-16	0.	.3369E-17	0.	-.2751E-17
129	.2693E-14	0.	.4164E-15	.5531E-17	0.	-.1154E-16	0.	.8476E-18	0.	-.6650E-18
130	.1060E-05	0.	.2774E-11	-.1365E-12	0.	.3482E-12	0.	.3544E-14	0.	-.6515E-14
131	.4109E-10	0.	.2304E-11	-.2952E-13	0.	.9489E-13	0.	-.6531E-15	0.	-.8926E-15
132	.4106E-11	0.	.8914E-12	.1150E-13	0.	-.1659E-13	0.	-.6723E-16	0.	-.2438E-15
133	.7922E-12	0.	.2014E-12	.4165E-14	0.	-.8162E-14	0.	.8265E-15	0.	-.7334E-15
134	.1776E-10	0.	.5124E-13	.1422E-14	0.	-.2685E-14	0.	.4277E-15	0.	-.3454E-15
135	.3218E-05	0.	.8134E-11	-.1291E-11	0.	.2627E-11	0.	.1373E-12	0.	-.1436E-12
136	.1375E-05	0.	.1974E-10	-.3444E-12	0.	.7271E-12	0.	.1210E-13	0.	-.2733E-13
137	.2132E-10	0.	.6484E-11	.1111E-12	0.	-.2056E-12	0.	.1917E-14	0.	-.8607E-14
138	.6041E-11	0.	.2234E-11	.6666E-13	0.	-.1385E-12	0.	.2173E-13	0.	-.1971E-13
139	.2025E-11	0.	.8704E-12	.3550E-13	0.	-.7403E-13	0.	.1646E-13	0.	-.1343E-13
140	.7602E-05	0.	.1524E-10	-.6579E-11	0.	.1106E-10	0.	.1454E-11	0.	-.1053E-11

Table A-3. (cont'd)

CASE	C00	C10	C01	C20	C11	C02	C30	C21	C12	C03
141	.3344E-05	0.	.340[illegible]-10	-.2186E-11	0.	.3216E-11	0.	.2787E-12	0.	-.2190E-12
142	.7018E-10	0.	.2694E-10	.4621E-12	0.	-.1105E-11	0.	.5979E-13	0.	-.8036E-13
143	.2650E-10	0.	.1256E-10	.4442E-12	0.	-.1020E-11	0.	.2296E-12	0.	-.2027E-12
144	.1101E-10	0.	.6554E-11	.3335E-12	0.	-.7324E-12	0.	.2224E-12	0.	-.1798E-12
145	.1606E-06	0.	.1094E-10	-.5274E-10	0.	.4418E-10	0.	.1454E-10	0.	-.6620E-11
146	.7486E-06	0.	.7952E-10	-.2295E-10	0.	.1536E-10	0.	.4903E-11	0.	-.1602E-11
147	.1965E-06	0.	.8094E-10	-.1777E-11	0.	-.2552E-11	0.	.1082E-11	0.	-.6184E-12
148	.9099E-10	0.	.4766E-10	.8545E-12	0.	-.4438E-11	0.	.1641E-11	0.	-.1275E-11
149	.4946E-10	0.	.3144E-10	.1597E-11	0.	-.6207E-11	0.	.1743E-11	0.	-.1358E-11
150	.8892E-11	0.	.1688E-12	-.1509E-14	0.	.2701E-14	0.	.1746E-16	0.	-.5065E-17
151	.3107E-11	0.	.7374E-13	-.4072E-15	0.	.7369E-15	0.	.6965E-17	0.	-.7988E-18
152	.1083E-12	0.	.9714E-14	.8618E-16	0.	-.8016E-16	0.	.4868E-18	0.	-.6230E-19
153	.7699E-14	0.	.7960E-15	.1150E-16	0.	-.1180E-16	0.	.8195E-18	0.	-.3406E-18
154	.6671E-15	0.	.7340E-16	.1481E-17	0.	-.1510E-17	0.	.1538E-18	0.	-.6219E-19
155	.6922E-10	0.	.1744E-11	-.7747E-13	0.	.1045E-12	0.	.5107E-15	0.	-.9567E-15
156	.2594E-10	0.	.1054E-11	-.1560E-13	0.	.2676E-13	0.	-.2631E-15	0.	-.1232E-15
157	.1996E-11	0.	.2944E-12	.6020E-14	0.	-.4305E-14	0.	-.3951E-17	0.	-.2494E-16
158	.2798E-12	0.	.4879E-13	.1539E-14	0.	-.1411E-14	0.	.2014E-15	0.	-.8543E-16
159	.4582E-13	0.	.9086E-14	.3884E-15	0.	-.3746E-15	0.	.7840E-16	0.	-.3215E-16
160	.2188E-06	0.	.5293E-11	-.7802E-12	0.	.8324E-12	0.	.2871E-13	0.	-.2164E-13

Table A-3. (cont'd)

CASE	C00	C10	C01	C20	C11	C02	C30	C21	C12	C03
161	.8696E-16	0.	.4726E-11	-.1994E-12	0.	.2352E-12	0.	-.1799E-14	0.	-.3751E-14
162	.1020E-10	0.	.2104E-11	.5819E-13	0.	-.4520E-13	0.	-.3860E-15	0.	-.9834E-15
163	.2131E-11	0.	.5336E-12	.2465E-13	0.	-.2355E-13	0.	.5065E-14	0.	-.2389E-14
164	.5185E-12	0.	.1517E-12	.9751E-14	0.	-.9546E-14	0.	.2984E-14	0.	-.1252E-14
165	.4963E-09	0.	.1054E-10	-.3978E-11	0.	.3512E-11	0.	.4383E-12	0.	-.1897E-12
166	.2082E-09	0.	.1424E-10	-.1270E-11	0.	.1028E-11	0.	.6997E-13	0.	-.4061E-13
167	.3291E-10	0.	.8607E-11	.2507E-12	0.	-.2441E-12	0.	.1118E-13	0.	-.1232E-13
168	.9159E-11	0.	.2956E-11	.1651E-12	0.	-.1743E-12	0.	.5356E-13	0.	-.2489E-13
169	.2964E-11	0.	.1135E-11	.9199E-13	0.	-.9494E-13	0.	.4026E-13	0.	-.1685E-13
170	.1020E-08	0.	.1284E-10	-.2913E-10	0.	.1327E-10	0.	.4472E-11	0.	-.1110E-11
171	.4512E-09	0.	.3276E-10	-.1206E-10	0.	.4454E-11	0.	.1378E-11	0.	-.2947E-12
172	.8937E-10	0.	.2566E-10	-.4120E-12	0.	-.7601E-12	0.	.2399E-12	0.	-.8864E-13
173	.3049E-10	0.	.1116E-10	.4329E-12	0.	-.7697E-12	0.	.3682E-12	0.	-.1558E-12
174	.1205E-10	0.	.5416E-11	.4697E-12	0.	-.5516E-12	0.	.3115E-12	0.	-.1270E-12
175	.2720E-09	.1578E-10	.1156E-10	.5485E-11	-.1559E-12	.3561E-12	-.7187E-12	.5277E-12	.1980E-12	-.5037E-13
176	.1297E-09	.2399E-10	.4186E-11	.1402E-11	.1095E-11	.2937E-12	-.6598E-13	.1196E-12	.9018E-13	-.1998E-13
177	.2856E-10	.1772E-10	.4276E-12	-.9756E-12	.9672E-12	.1465E-12	-.3867E-13	-.8273E-13	.6388E-13	-.1626E-15
178	.1225E-10	.9099E-11	.1516E-12	-.8243E-12	.3453E-12	.8613E-13	-.1915E-12	-.5468E-13	.6920E-13	.9024E-15
179	.6524E-11	.5347E-11	.7677E-13	-.6015E-12	.1224E-12	.3518E-13	-.1953E-12	-.2713E-13	.5894E-13	.5096E-15
180	.2613E-08	.2322E-09	.1107E-09	.1553E-09	-.6888E-10	.1080E-10	-.5963E-10	.3332E-10	.2022E-10	-.5270E-11

Table A-3. (cont'd)

CASE	C00	C10	C01	C20	C11	C02	C30	C21	C12	C03
181	.1[illegible]E-0[illegible]	.4751E-05	.3122E-10	.3802E-10	.1113E-10	.9970E-11	-.1613E-11	.9892E-11	.8802E-11	-.2629E-11
182	.5618E-05	.6454E-05	-.1228E-11	-.6693E-10	.4223E-10	.1016E-10	-.7226E-11	-.6859E-11	.9950E-11	-.6759E-12
183	.4365E-09	.6187E-05	-.4126E-11	-.1099E-09	.2922E-10	.1290E-10	-.5109E-10	-.9812E-11	.1901E-10	-.3431E-12
184	.4677E-06	.7276E-05	-.6419E-11	-.1599E-09	.1806E-10	.1541E-10	-.1918E-09	-.8957E-11	.3127E-10	-.3566E-12
185	.3900E-05	.6247E-05	.2036E-09	.4519E-05	-.2412E-09	.3568E-10	-.2244E-05	.1159E-05	.8173E-10	-.2120E-10
186	.2194E-04	.1264E-04	.4033E-10	.1151E-09	.1971E-10	.3279E-10	.7986E-11	.3933E-10	.3510E-10	-.1154E-10
187	.6469E-05	.9503E-05	-.1268E-10	-.1271E-09	.6969E-10	.2034E-10	-.1459E-10	-.1282E-10	.2424E-10	-.2187E-11
188	.3511E-05	.6042E-05	-.9822E-11	-.1307E-09	.2779E-10	.1481E-10	-.7458E-10	-.1163E-10	.2867E-10	-.8674E-12
189	.2362E-05	.4428E-05	-.7839E-11	-.1182E-09	.8369E-11	.1179E-10	-.9363E-10	-.5817E-11	.2937E-10	-.5981E-12
190	.1292E-05	.3815E-11	.7266E-11	.6191E-12	.3233E-12	.2493E-12	-.3214E-11	.6692E-11	.3059E-11	-.2248E-13
191	.5706E-10	.3995E-11	.2574E-11	.1785E-12	.3289E-12	.1507E-12	-.7205E-14	.1438E-11	.1677E-11	-.8383E-14
192	.7390E-11	.1849E-11	.1423E-12	-.4692E-13	.1589E-12	.3554E-13	-.1541E-14	-.7220E-14	.6908E-14	.7763E-16
193	.1709E-11	.5144E-12	.1986E-13	-.2524E-13	.4075E-13	.1263E-13	-.3287E-14	-.2819E-14	.4107E-14	.1837E-15
194	.4798E-12	.1816E-12	.3854E-14	-.1078E-13	.1135E-13	.4470E-14	-.1880E-14	-.9163E-15	.1989E-14	.7221E-16
195	.4156E-05	.1482E-10	.2886E-10	.4492E-11	-.2594E-13	.1692E-11	-.5992E-12	.8794E-12	.5543E-12	-.4263E-12
196	.9430E-09	.4285E-10	.7747E-10	.1783E-10	-.6761E-11	.6609E-11	-.3199E-11	.4984E-11	.3635E-11	-.2740E-11
197	.1793E-04	.1066E-05	.1592E-09	.5078E-10	-.3150E-10	.2081E-10	-.1226E-10	.1782E-10	.1500E-10	-.1081E-10
198	.3051E-04	.2244E-05	.2826E-09	.1215E-05	-.9975E-10	.5329E-10	-.3707E-10	.5235E-10	.4662E-10	-.3365E-10
199	.4766E-04	.4207E-05	.4514E-09	.2559E-05	-.2230E-09	.1140E-09	-.9249E-10	.1272E-05	.1229E-09	-.8948E-10
200	.7035E-04	.7456E-05	.6704E-09	.4606E-09	-.4998E-09	.2226E-09	-.2156E-05	.2771E-05	.3098E-09	-.2087E-09

Table A-3. (cont'd)

CASE	C00	C10	C01	C20	C11	C02	C30	C21	C12	C03
201	.5982E-08	.1573E-08	.1074E-09	.1328E-09	.1753E-10	.1845E-09	-.1929E-10	.8850E-10	.1538E-09	-.1157E-09
202	.2244E-08	.2227E-08	-.1160E-09	-.2341E-09	.2830E-09	.1518E-09	-.4141E-10	-.5198E-10	.1894E-09	-.4730E-10
203	.2151E-08	.2582E-08	-.1697E-09	-.4655E-09	.2647E-09	.2453E-09	-.2304E-09	-.9213E-10	.3512E-09	-.3730E-10
204	.2482E-08	.5253E-08	-.2411E-09	-.7787E-09	.2507E-09	.3489E-09	-.5068E-09	-.1063E-09	.6233E-09	-.4120E-10
205	.9983E-08	.1219E-07	.1022E-08	.8412E-09	-.1966E-08	.4024E-09	-.4549E-09	.5494E-09	.6843E-09	-.4213E-09
206	.1497E-14	.4732E-14	.2799E-12	.5345E-14	.1172E-13	.6748E-14	-.1958E-15	.3992E-15	.5350E-15	-.1438E-15
207	.9887E-14	.6087E-11	.2755E-11	.2156E-12	.2274E-12	.2717E-12	-.1767E-13	.2158E-13	.3431E-13	-.1210E-13
208	.4273E-10	.2173E-11	.2366E-11	.1236E-12	.1901E-12	.7774E-13	-.6679E-14	.1179E-13	.8166E-14	-.3353E-14
209	.2364E-11	.4690E-11	.4446E-12	.1340E-12	.3923E-13	-.8944E-14	-.2037E-16	.1893E-14	-.1370E-14	-.2826E-15
210	.2282E-12	.2225E-14	.5066E-13	.1754E-14	.4227E-14	-.1977E-14	.1611E-16	.4333E-15	-.2259E-15	-.2134E-15
211	.2659E-11	.1085E-15	.6452E-14	.2552E-15	.4931E-15	-.3485E-15	.2781E-17	.8424E-16	-.3076E-16	-.4920E-16
212	.3152E-09	.2494E-10	.8473E-11	.1386E-11	.7067E-12	.2139E-11	-.3196E-12	.2769E-12	.4185E-12	-.1694E-12
213	.7671E-09	.6731E-10	.2166E-10	.5231E-11	-.9567E-12	.8636E-11	-.2121E-11	.1843E-11	.2393E-11	-.1046E-11
214	.3350E-09	.2110E-10	.7844E-10	.3694E-11	.3631E-11	.2427E-11	-.9496E-12	.1031E-11	.6029E-12	-.2089E-12
215	.7265E-10	.1169E-11	.2835E-10	.1555E-11	.3740E-11	-.1162E-11	-.1231E-12	.5677E-12	-.2663E-12	-.7739E-13
216	.2743E-10	.9605E-12	.1316E-10	.6116E-12	.1517E-11	-.1030E-11	-.2663E-13	.4769E-12	-.1880E-12	-.2096E-12
217	.1242E-10	-.3611E-12	.6895E-11	.4733E-12	.7460E-12	-.7273E-12	-.7752E-14	.3578E-12	-.1026E-12	-.1947E-12
218	.1363E-08	.1430E-09	.5505E-10	.1612E-10	-.1229E-10	.2426E-10	-.8594E-11	.7991E-11	.8952E-11	-.4335E-11
219	.2283E-08	.2616E-09	.1173E-09	.4216E-10	-.4330E-10	.5702E-10	-.2622E-10	.2527E-10	.2689E-10	-.1352E-10
220	.1172E-08	.7273E-10	.2345E-09	.3173E-10	.1044E-10	.1497E-10	-.1318E-10	.1381E-10	.8033E-11	-.2436E-11

Table A-3. (cont'd)

CASE	C00	C10	C01	C20	C11	C02	C30	C21	C12	C03
221	.3991E-09	-.4840E-12	.2324E-09	.1986E-10	.2932E-10	-.1515E-10	-.3230E-11	.1125E-10	-.2734E-11	-.1884E-11
222	.2319E-09	-.4569E-11	.1634E-09	.1556E-10	.1780E-10	-.1905E-10	-.1530E-11	.1336E-10	-.3091E-11	-.5834E-11
223	.1616E-09	-.4953E-11	.1284E-09	.1360E-10	.1106E-10	-.1986E-10	-.9935E-12	.1486E-10	-.2304E-11	-.7881E-11
224	.3550E-08	.4382E-09	.2054E-09	.8651E-10	-.1066E-09	.1210E-09	-.6915E-10	.6676E-10	.6532E-10	-.3390E-10
225	.5218E-08	.6736E-09	.3524E-09	.1692E-09	-.2512E-09	.2278E-09	-.1619E-09	.1639E-09	.1445E-09	-.7652E-10
226	.2640E-08	.1565E-09	.7994E-09	.1353E-09	.2214E-10	.6266E-10	-.8714E-10	.8773E-10	.4542E-10	-.1054E-10
227	.1307E-08	-.4006E-10	.9944E-09	.1144E-09	.1474E-09	-.8456E-10	-.2925E-10	.8710E-10	-.2047E-10	-.1319E-10
228	.1013E-08	-.5946E-10	.9270E-09	.1195E-09	.1218E-09	-.1419E-09	-.1678E-10	.1344E-09	-.3105E-10	-.5715E-10
229	.9396E-09	-.7307E-10	.9726E-09	.1391E-09	.1023E-09	-.1973E-09	-.1657E-10	.1977E-09	-.3195E-10	-.1034E-09
230	.2430E-08	.7631E-09	.4364E-10	.1071E-09	-.3679E-10	.2674E-10	-.1335E-09	.4263E-10	.2770E-10	-.4612E-11
231	.6024E-10	.4760E-11	.1314E-11	.1343E-12	.1391E-12	.7535E-13	-.1047E-13	.1011E-13	.1192E-13	-.2442E-14
232	.2498E-10	.1682E-11	.9321E-12	.7355E-13	.9328E-13	.2114E-13	-.3845E-14	.5551E-14	.3232E-14	-.7990E-15
233	.2018E-11	.7079E-13	.2674E-12	.1218E-13	.2542E-13	-.4068E-14	.4090E-16	.1282E-14	-.5714E-15	-.1018E-15
234	.2867E-12	.6681E-14	.4426E-13	.2374E-14	.4163E-14	-.1310E-14	.2799E-16	.4149E-15	-.1437E-15	-.1033E-15
235	.4860E-13	.8356E-15	.8164E-14	.5142E-15	.7273E-15	-.3415E-15	.6622E-17	.1194E-15	-.2978E-16	-.3462E-16
236	.4530E-09	.5351E-10	.1004E-10	.3877E-11	.9613E-12	.2621E-11	-.1422E-11	.7280E-12	.8446E-12	-.2127E-12
237	.2051E-09	.1666E-10	.1427E-10	.2557E-11	.1891E-11	.7413E-12	-.6213E-12	.4171E-12	.2252E-12	-.5662E-13
238	.3276E-14	.7383E-12	.8356E-11	.8009E-12	.1353E-11	-.2436E-12	-.6617E-13	.1841E-12	-.6030E-13	-.1552E-13
239	.9403E-11	.2043E-13	.2852E-11	.3035E-12	.4486E-12	-.1654E-12	-.1411E-13	.1151E-12	-.3211E-13	-.2567E-13
240	.3407E-11	-.3781E-13	.1084E-11	.1296E-12	.1530E-12	-.8770E-13	-.4164E-14	.6372E-13	-.1546E-13	-.1741E-13

Table A-3. (cont'd)

CASE	C00	C10	C01	C20	C11	C02	C30	C21	C12	C03
241	.1440E-04	.2165E-05	.4305E-10	.2884E-10	-.1041E-10	.1772E-10	-.1809E-10	.1032E-10	.9484E-11	-.2696E-11
242	.7001E-05	.6300E-10	.8277E-10	.2073E-10	.6702E-11	.6706E-11	-.8776E-11	.5858E-11	.2834E-11	-.7216E-12
243	.1777E-05	.1955E-11	.6697E-10	.9702E-11	.1063E-10	-.3135E-11	-.1639E-11	.3634E-11	-.6439E-12	-.3412E-12
244	.7551E-10	-.7077E-12	.3479E-10	.5542E-11	.5020E-11	-.3029E-11	-.5875E-12	.3168E-11	-.3597E-12	-.6954E-12
245	.3696E-10	-.9291E-12	.2004E-10	.3560E-11	.2442E-11	-.2377E-11	-.2810E-12	.2614E-11	-.3368E-12	-.6900E-12
246	.3258E-04	.6021E-05	.1194E-09	.1135E-09	-.7214E-10	.7060E-10	-.1082E-05	.6465E-10	.5140E-10	-.1676E-10
247	.1673E-04	.1662E-05	.2814E-09	.8673E-10	.2092E-10	.1937E-10	-.5560E-10	.3584E-10	.1565E-10	-.3482E-11
248	.5686E-05	.2456E-12	.2869E-09	.5481E-10	.5365E-10	-.1785E-10	-.1356E-10	.2762E-10	-.4932E-11	-.2382E-11
249	.3214E-05	-.9039E-11	.1983E-09	.4164E-10	.3420E-10	-.2276E-10	-.6360E-11	.3142E-10	-.5656E-11	-.6738E-11
250	.2152E-05	-.1043E-10	.1523E-09	.3571E-10	.2234E-10	-.2373E-10	-.3905E-11	.3433E-10	-.4533E-11	-.8957E-11
251	6.2185E-09	2.0625E-09	2.0285E-10	3.5811E-11	-4.370E-10	2.3895E-10	-7.2805E-10	4.2835E-10	3.7585E-10	-8.6105E-11
252	3.3565E-09	6.3875E-10	7.0425E-10	1.321E-10	-4.4265E-11	7.150E-11	-3.7265E-10	2.2435E-10	1.4945E-10	-2.2325E-11
253	1.4455E-09	1.0525E-11	8.9135E-10	1.3915E-10	1.4855E-10	-6.925E-11	-9.4425E-11	1.5455E-10	-4.0135E-12	-1.4765E-11
254	1.0275E-09	-8.6295E-11	7.7605E-10	2.1495E-10	1.1955E-10	-1.1285E-10	-4.2655E-11	1.3755E-10	-2.7485E-11	-4.243 -11
255	8.6475E-10	-1.4505E-10	7.5095E-10	2.4615E-10	9.435E-11	-1.4805E-10	-1.9535E-11	2.5965E-10	-3.5635E-11	-6.8495E-11
256	8.9155E-09	2.6045E-09	7.6195E-10	2.0645E-11	-1.2475E-09	7.6355E-10	-1.0315E-09	1.0945E-09	1.1035E-09	-4.0275E-10
257	5.6375E-09	8.9735E-10	2.0445E-09	1.9485E-10	-1.7945E-10	2.3695E-10	-5.7585E-10	5.7545E-10	4.5625E-10	-8.4145E-11
258	3.3475E-09	-1.0355E-10	3.1225E-09	4.2585E-10	4.1295E-10	-3.2795E-10	-1.8785E-10	5.1015E-10	-3.4035E-11	-5.6135E-11
259	3.3035E-09	-3.9245E-10	3.6675E-09	5.417E-10	4.355E-10	-7.0345E-10	-1.0635E-10	8.6935E-10	-1.8475E-10	-3.6145E-10
260	3.8765E-09	-7.4665E-10	4.4385E-09	9.9795E-10	4.3805E-10	-1.2325E-09	-6.0125E-11	1.5315E-09	-2.9575E-10	-7.5265E-10

APPENDIX B

MODE-ONE STRESS INTENSITY FACTOR CALCULATIONS

1. INTRODUCTION

Tables 4 and 5 and Tables 7 and 8 in an earlier section of this report list dimensionless stress intensity magnification factors for corner and surface cracks, respectively, at holes in plates. These magnification factors are shown in the interest of brevity, for 30^{o} increments along the crack border. It is entirely possible that at some future date similar information for other locations might be needed. This appendix describes two computer programs, one written in FORTRAN and the other in BASIC, which generate mode-one stress intensity factors, K_I, at one degree increments of parametric angle along the crack border.

2. PROGRAM DESCRIPTION

Programs KFRTN and KBSC, whose listings are found in Tables B-1 and B-2 respectively, perform identical functions. The difference, of course, is the computer language used. Program KFRTN is in FORTRAN and KBSC is in BASIC and this latter program was written and tested on the Hewlett-Packard series of desktop computers. Both programs are structured in a standard fashion. The first section reads and writes input parameters. The second section determines the parametric angles for which K_I will be calculated along the crack border depending upon the crack location and shape. The third and final section performs the lengthy algebraic calculation to arrive at K_I.

3. PROGRAM INPUT

Table B-3 lists required variable inputs determined for the particular case being considered. Figure B-1 graphically depicts these parameters in more detail. The authors suggest that any user of these programs exercise special care to be absolutely certain these parameters are correctly input (sketches similar to those of Figure B-1 are particularly helpful).

The user should also be aware of certain values fixed in the software which must remain as shown. All calculations are for a Poissons Ratio of 0.25 and a Modulus of Rigidity of 12×10^6 psi. Stress intensity factors obtained from the stress function coefficients are given in Table A-3 for specific loadings. For the remote tension cases, the applied load was 1 psi. For the crack face pressure problems, the applied load is $p(x/R) = A_o, A_1(x/R), A_2(x/R)^2, A_3(x/R)^4$, where $A_0 = A_1 = A_2 = A_3 = 1$ and R = 0.5. Other loadings and hole diameters can be considered by scaling the resulting stress intensity factors in an appropriate manner (multiply by desired remote stress, pressure load A_n, and/or relate crack dimensions through a/c and a/t). In all cases, one must maintain 2R = T.

4. PROGRAM OUTPUT

Table B-4 shows a sample output of Program KBSC (output of KFRTN is similar). The mode-one stress intensity factor, K_I, is printed for increments of parametric angle, ϕ, where this angle is always measured from the crack semi-minor axis as shown in Figures 5 and 6. For the corner crack, K_I will be calculated for 0 to 90° in one degree increments but for the surface crack K_I will be calculated for -90° to +90° (all along the crack border) in two degree increments. Note that in the outputs of programs KBSC and KFRTN, the parametric angle ϕ is always measured from the semi-minor axis, while in Tables 4 and 5, ϕ is always defined as the distance from the front surface for the corner cracks as in Fig. 5. Thus, for a/c > 1.0, both the tabulated and computer program output have the same definition for ϕ, while for a/c < 1.0, the angles are complementary. Since a/c always exceeds 1.0 for the semielliptical cracks considered, there is no inconsistency in the two definitions for ϕ.

Table B-1 Program KFRTN Listing

```
C     THIS PROGRAM CALCULATES MODE I STRESS INTENSITY FACTORS AT ONE
C     DEGREE INCREMENTS OF ELLIPTICAL ANGLE ALONG THE BORDER OF A
C     SEMIELLIPTICAL CRACK INTERSECTING A FASTENER HOLE IN A FLAT PLATE
C
C
C     INPUTS ARE
C
C     NAXIS = CRACK ORIENTATION(SEE EXPLANATORY FIGURES)
C     A = CRACK SEMI-MAJOR AXIS
C     B = CRACK SEMI-MINOR AXIS
C     D1 = DISTANCE FROM PLATE CENTER TO CRACK CENTER(SEE FIGURES)
C     C(I) = STRESS FUNCTION COEFFICIENTS, INPUT IN ORDER OF TABLE
C
C
C     OUTPUTS ARE
C
C     ANGLE = ELLIPTICAL OR PARAMETRIC ANGLE FROM CRACK MINOR AXIS
C     KI = MODE ONE STRESS INTENSITY FACTOR FOR ONE PSI REMOTE STRESS
C
      DIMENSION C(10)
      G= 12000000.
      PI=3.14159
      T1=1.0
      READ(5,1) NAXIS,A,B,D1
      WRITE(6,2) NAXIS
      WRITE(6,3) A
      WRITE(6,4) B
      WRITE(6,5) D1
      READ(5,6) (C(I),I=1,8)
      READ(5,6) (C(I),I=9,10)
      WRITE(6,11)
      WRITE(6,7) (C(I),I=1,10)
      WRITE(6,8)
C     DETERMINE ANGLES FOR WHICH STRESS INTENSITY FACTORS WILL BE
C     CALCULATED.
C
      OPP=.5*T1+D1
      OPP=AMAX1(OPP,-A)
      OPP=AMIN1(OPP,A)
      T1=ASIN(OPP/A)
      OPP=.5*T1-D1
      OPP=AMAX1(OPP,-A)
      OPP=AMIN1(OPP,A)
      T2=ASIN(OPP/A)
      DT=(T2+T1)*2./PI
      T1=T1*180./PI
      IF(NAXIS-2)10,20,30
   30 PRINT 1000, NAXIS
 1000 FORMAT(1X,'NAXIS NOT 1 OR 2',I10 )
   20 CONTINUE
      T1=T1-90.
      GO TO 40
   10 CONTINUE
   40 CONTINUE
      DO 100 I=1,91
      ANG=(I-1)*DT-T1
      CALC=-ANG+90.
      TH=CALC*PI/180.
      AKI=8.*G/(A+B)*SQRT(PI/(A*B))*(A*A*(SIN(TH))**2+
     1B*B*((COS(TH))**2)**.25*(C(1)+C(3)*SIN(TH)/B-4.*
     2C(4)*(COS(TH))**2/(A*A)-4.*C(6)*(SIN(TH))**2/(B*B)
     3-4.*C(8)*(COS(TH))**2*SIN(TH)/(A*A*B)-4.*C(10)*
     4(SIN(TH))**3/B**3+C(2)*COS(TH)/A+C(5)*COS(TH)*SIN(TH)/(A*B)-4.*
     5C(7)*(COS(TH)/A)**3-4.*C(9)*(COS(TH)/A)*(SIN(TH)/B)**2)
      WRITE(6,9) ANG,AKI
      ANG=0.0
      CALC=0.0
      AKI=0.0
      TH=0.0
  100 CONTINUE
    1 FORMAT(I10,3F10.4)
    2 FORMAT(1H0,'NAXIS =',I2,/)
    3 FORMAT(1H0,'CRACK SEMI-MAJOR AXIS =',F5.2,/)
    4 FORMAT(1H0,'CRACK SEMI-MINOR AXIS =',F5.2,/)
    5 FORMAT(1H0,'DISTANCE TO CRACK CENTER, D1 =',F5.2,//)
    6 FORMAT(8E10.4)
    7 FORMAT(1DE13.4)
    8 FORMAT(//,6X,'ANGLE',6X,'KI',/)
    9 FORMAT(F10.1,F10.3)
   11 FORMAT(1H0,'STRESS FUNCTION COEFFICIENTS, C(1) TO C(10)',/)
      STOP
      END
```

Table B-2. Program KBSC Listing

```
10 DIM A[5],B[5],E[4],F[4],C[10],N[10]
20 PRINT "THIS PROGRAM CALCULATES MODE ONE STRESS INTENSITY FACTORS",LIN2
30 FOR I=1 TO 10
40 C[I]=0
50 NEXT I
60 DISP "INPUT CRACK SEMI-MAJOR AND SEMI-MINOR AXES:A,B";
70 INPUT A,B
80 PRINT LIN2,"SEMI-MAJOR AXIS =";A;"SEMI-MINOR AXIS =";B
90 N[1]=0
100 N[2]=0.1
110 N[3]=0.01
120 N[4]=0.2
130 N[5]=0.11
140 N[6]=0.02
150 N[7]=0.3
160 N[8]=0.21
170 N[9]=0.12
180 N[10]=0.03
190 DISP "INPUT STRESS FUNCTION COEFFICIENTS"
200 WAIT 3000
210 PRINT LIN2,"C00 TO C03",LIN1
220 FOR I=1 TO 10
230 FIXED 2
240 DISP "C",N[I],"=";
250 STANDARD
260 INPUT C[I]
270 WRITE (2,280)C[I]
280 FORMAT E13.3
290 NEXT I
300 DISP "FOR CORRECTIONS ENTER 1, IF NO CORRECTIONS ENTER 0";
310 INPUT K
320 IF K=1 THEN 340
330 GOTO 360
340 DISP "ENTER COEFFICIENT NUMBER, C(XX)=?, AND PRESS CONT-EXECUTE";
350 STOP
360 DISP "NAXIS =";
370 INPUT N2
380 G=12000000
390 DISP "DISTANCE TO CRACK CENTER = ";
400 INPUT D1
410 T=1
420 PRINT LIN1,"NAXIS = ";N2
430 PRINT "G = ";G
440 PRINT "DISTANCE TO THE CRACK CENTER = ";D1
450 PRINT "PLATE THICKNESS = ";T
460 PRINT LIN2,"ANGLE = PARAMETRIC ANGLE FROM MINOR AXIS",LIN1
470 PRINT "KI = MODE-ONE STRESS INTENSITY FACTOR",LIN1
480 PRINT LIN1,"ANGLE";SPA8;"KI";LIN2;
```

Table B-2. (cont'd)

```
490 O1=0.5*T+D1
500 A9=-A
510 IF O1<A9 THEN 530
520 GOTO 540
530 O1=A9
540 IF O1>A THEN 560
550 GOTO 570
560 O1=A
570 O2=O1/A
580 IF O2=1 THEN 600
590 GOTO 620
600 T1=PI/2
610 GOTO 630
620 T1=ATN(O2/SQR(1-O2↑2))
630 O1=0.5*T-D1
640 IF O1<A9 THEN 660
650 GOTO 670
660 O1=A9
670 IF O1>A THEN 690
680 GOTO 700
690 O1=A
700 O2=O1/A
710 IF O2=1 THEN 730
720 GOTO 750
730 T2=PI/2
740 GOTO 760
750 T2=ATN(O2/SQR(1-O2↑2))
760 D2=(T2+T1)*2/PI
770 T1=T1*180/PI
780 IF N2=2 THEN 800
790 GOTO 810
800 T1=T1-90
810 FOR I=1 TO 91
820 A3=(I-1)*D2-T1
830 A4=-A3+90
840 A5=A4*PI/180
850 F3=8*G/(A*B)*SQR(PI/(A*B))*(A*A*(SIN(A5))↑2+B*B*(COS(A5))↑2)↑0.25
860 F4=C[1]+C[3]*SIN(A5)/B-4*C[4]*(COS(A5))↑2/(A*A)
870 F5=-4*C[6]*(SIN(A5))↑2/(B*B)-4*C[8]*(COS(A5))↑2*SIN(A5)/(A*A*B)
880 F6=-4*C[10]*(SIN(A5))↑3/B↑3+C[2]*COS(A5)/A
890 F7=C[5]*COS(A5)*SIN(A5)/(A*B)-4*C[7]*(COS(A5)/A)↑3
900 F8=-4*C[9]*(COS(A5)/A)*(SIN(A5)/B)↑2
910 K9=F3*(K4+F5+F6+K7+K8)
920 WRITE (2,930)A3,K9
930 FORMAT F4.0,F12.4
940 NEXT I
950 END
```

Table B-3 Input List

Input	Description	Determined From
NAXIS	Define the crack orientation with respect to the plate	Figure B-1
A	Crack semi-major axis	Table A-1 or A-2
B	Crack semi-minor axis	Table A-1 or A-2
D1	Locates the crack center with respect to the plate	Figure B-1
C(I)	Coefficients to calculate K_I where C(1) = C00, ..., C(10) = C03	Table A-3 (reading from left to right)

Corner Crack ($a/c \leq 0.9$, $2R = T = 1$.

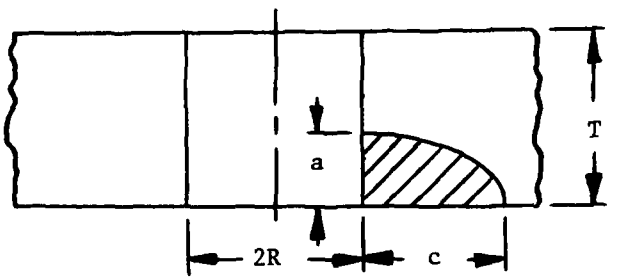

Input: A = c
B = a
D1 = + 0.5
NAXIS = 2

Corner Crack ($a/c \geq 1.1$, $2R = T = 1$.

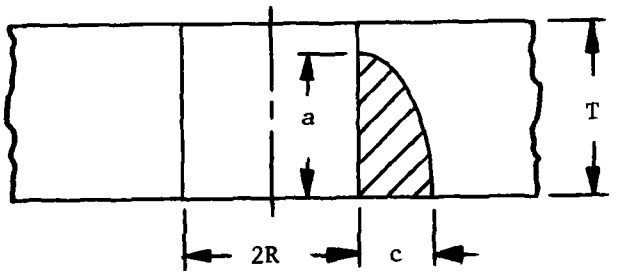

Input: A = a
B = c
D1 = - 0.5
NAXIS = 1

Surface Crack ($c/a \leq 0.9$, $2R = T = 1$.

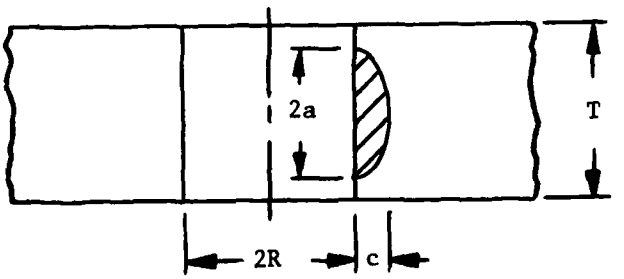

Input: A = a
B = c
D1 = 0.0
NAXIS = 1

Fig. B-1 Input Description

Table B-4. Sample Output, Program KBSC

```
THIS PROGRAM CALCULATES MODE ONE SINGLE INTENSITY FACTORS


SEMI MAJOR AXIS = 1     SEMI-MINOR AXIS = 0.5

RUN ID: C03

      3.797E-09
     -6.296E-10
      2.137E-10
     -1.347E-10
      9.206E-11
     -6.931E-11
      5.270E-11
     -4.126E-11
      3.257E-11
     -2.107E-11

NO.(I) =  2
G     1.2000000
DISTANCE TO THE ANCHOR CENTER     0.5
FIXED THICKNESS  =  1

NO.J   = PARAMETRIC ANGLE FROM MINOR AXIS

J.    MODE-ONE STRESS INTENSITY FACTOR


 N.J          F1


      0        2.1041
      1        2.0548
      2        2.0134
      3        2.0067
      4        2.0531
      5        2.1033
      .          .
      .          .
      .          .
     24        1.1121
     25        1.0920
     26        1.0771
     27        1.0714
     28        1.0701
     29        1.0732
```

APPENDIX C

CRACK OPENING DISPLACEMENT CALCULATIONS

1. INTRODUCTION

Crack opening displacements can be easily determined using input similar to those for the mode-one stress intensity factor calculations of Appendix B. Reference 10 fully describes the formulation of a lengthy yet simple algebraic expression which results in crack opening displacements. This appendix describes a computer program which will generate such displacements at certain locations on the crack plane.

2. PROGRAM DESCRIPTION AND INPUT

Computer program COD (listed in Table C-1) is written in BASIC on a Hewlett-Packard desktop computer. The derivation of the algebraic expression which yields crack opening displacement includes A, B, and C(I) which are exactly as described in Appendix B for Programs KFRTN and KBSC.

3. PROGRAM OUTPUT

Program COD output includes crack opening displacements calculated and printed for specific points along rays at 10^{o} increments of parametric angle, Φ, over 90^{o} of the crack where Φ is measured from the crack major axis. Figure C-1 depicts a few of these points for clarity. Each ray, whose length might be called r_i, has output points

$$0.0r_i,\ 0.1r_i,\ \ldots,\ 0.9r_i,\ 0.95r_i,\ 0.98r_i\ .$$

These points coincide with the description required for Benchmark Problems and an example can be found in Reference 3.

Table C-2 shows a sample output from Program COD. The coordinates of each point are described in terms of x and y (Figure C-1) rather than r_i. As with the Appendix B calculations, for the remote loading cases the uniform remote tension was one psi.

Table C-1. Program COD Listing

```
10 DIM X[12],Y[12],W[12],C[10],E[10],N[10]
20 PRINT "THIS PROGRAM CALCULATES CRACK OPENING DISPLACEMENTS",LIN2
30 FOR I=1 TO 10
40 E[I]=0
50 NEXT I
60 DISP "INPUT CRACK SEMI-MAJOR AND SEMI-MINOR AXES:A,B";
70 INPUT A,B
80 PRINT LIN2,"SEMI-MAJOR AXIS =";A;"SEMI-MINOR AXIS =";B
90 U=0.25
100 PRINT LIN2,"POISSON'S RATIO =";U;LIN2
110 N[1]=0
120 N[2]=0.1
130 N[3]=0.01
140 N[4]=0.2
150 N[5]=0.11
160 N[6]=0.02
170 N[7]=0.3
180 N[8]=0.21
190 N[9]=0.12
200 N[10]=0.03
210 DISP "INPUT STRESS FUNCTION COEFFICIENTS"
220 WAIT 3000
230 PRINT LIN2,"C00 TO C03",LIN1
240 FOR I=1 TO 10
250 FIXED 2
260 DISP "C",N[I],"=";
270 STANDARD
280 INPUT C[I]
290 WRITE (2,300)C[I]
300 FORMAT E13.4
310 NEXT I
320 DISP "FOR CORRECTIONS ENTER 1, IF NO CORRECTIONS ENTER 0";
330 INPUT K
340 IF K=1 THEN 360
350 GOTO 380
360 DISP "ENTER COEFFICIENT NUMBER, C(XX)=?, AND PRESS CONT-EXECUTE";
370 STOP
380 A1=(A↑2)*(B↑2)
390 A2=(A↑2)*(B↑4)
400 A3=(A↑4)*(B↑6)
410 A4=(A↑2)*(B↑6)
420 A5=(A↑4)*(B↑8)
430 A6=(A↑2)*(B↑8)
440 A7=(A↑4)*(B↑2)
450 A8=(A↑4)*(B↑4)
460 A9=(A↑6)*(B↑6)
```

Table C-1. (cont'd)

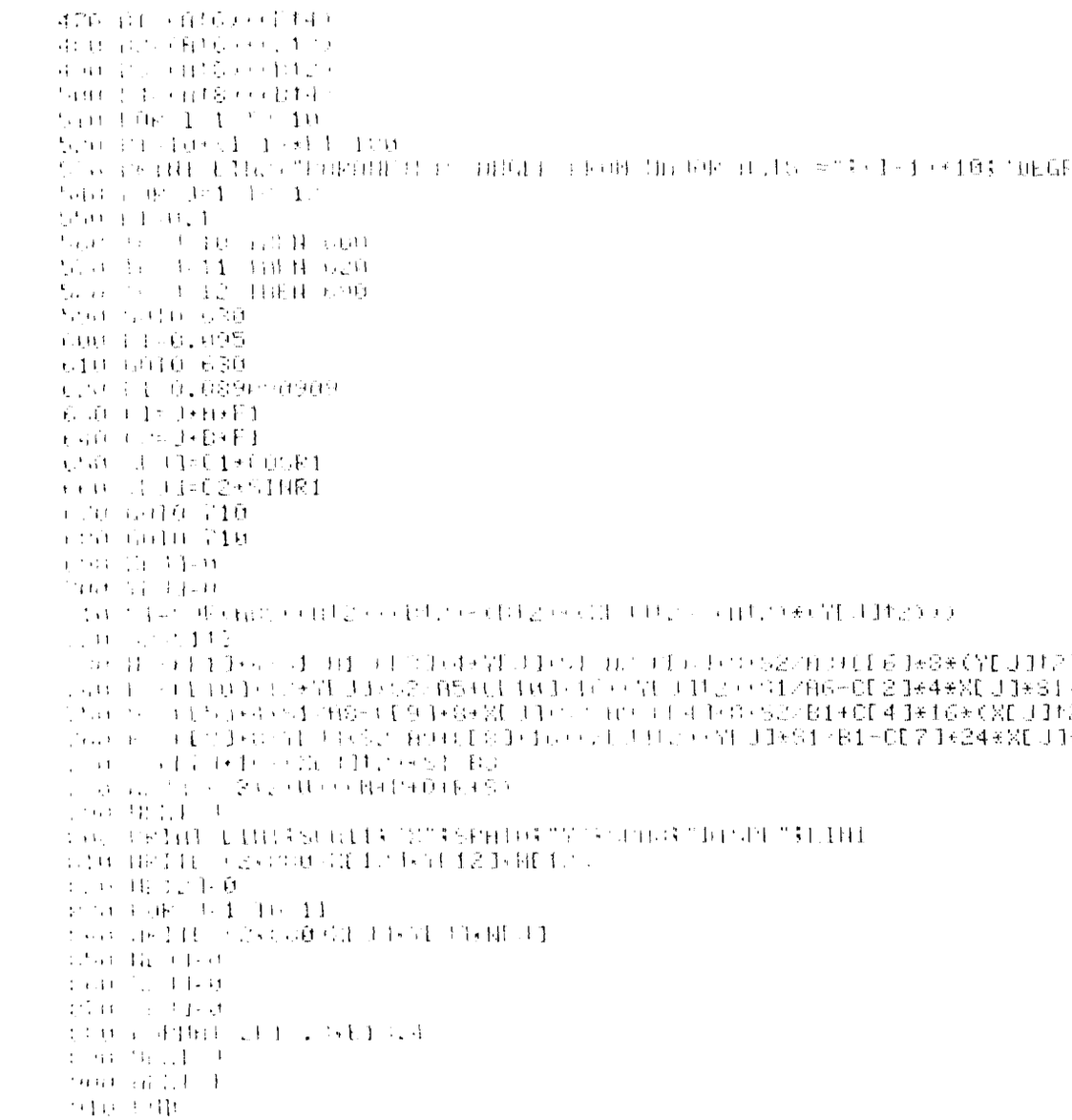

Table C-2. Sample Output, Program COD

```
THIS PROGRAM CALCULATES CRACK OPENING DISPLACEMENTS


SEMI-MAJOR AXIS = 1      SEMI-MINOR AXIS = 0.5

POISSON'S RATIO = 0.25


COD TO COD

   3.7970E-09
   6.2964E-10
   3.1370E-10
   4.3470E-10
  -2.2960E-10
   3.3510E-11
  -2.2700E-10
   1.1060E-10
   8.2570E-11
  -2.1070E-11

PARAMETRIC ANGLE FROM MAJOR AXIS = 0     DEGREES

          X              Y            DISP.

      0.000          0.000      4.8164E 00
      0.100          0.000      4.7611E 00
      0.200          0.000      4.6163E 00
      0.300          0.000      4.3890E 00
      0.400          0.000      4.0860E 00
      0.500          0.000      3.7140E 00
      0.600          0.000      3.2775E 00
      0.700          0.000      2.7763E 00
      0.800          0.000      2.2096E 00
      0.900          0.000      1.5798E-00
      0.950          0.000      1.2436E-00
      0.980          0.000      6.4335E 00
```

Table C-2. (cont'd)

PARAMETRIC ANGLE FROM MAJOR AXIS = 10 DEGREES

X	Y	DISPL
0.000	0.000	4.8164E-08
0.098	0.009	4.7697E-08
0.197	0.017	4.6336E-08
0.295	0.026	4.4134E-08
0.394	0.035	4.1150E-08
0.492	0.043	3.7436E-08
0.591	0.052	3.3035E-08
0.689	0.061	2.7949E-08
0.788	0.069	2.2075E-08
0.886	0.078	1.4951E-08
0.936	0.082	1.0308E-08
0.965	0.085	6.4134E-09
⋮	⋮	⋮

PARAMETRIC ANGLE FROM MAJOR AXIS = 90 DEGREES

X	Y	DISPL
0.000	0.000	4.8164E-08
0.000	0.050	4.8380E-08
0.000	0.100	4.8082E-08
0.000	0.150	4.7235E-08
0.000	0.200	4.5783E-08
0.000	0.250	4.3639E-08
0.000	0.300	4.0662E-08
0.000	0.350	3.6614E-08
0.000	0.400	3.1031E-08
0.000	0.450	2.2743E-08
0.000	0.475	1.6365E-08
0.000	0.490	1.0458E-08

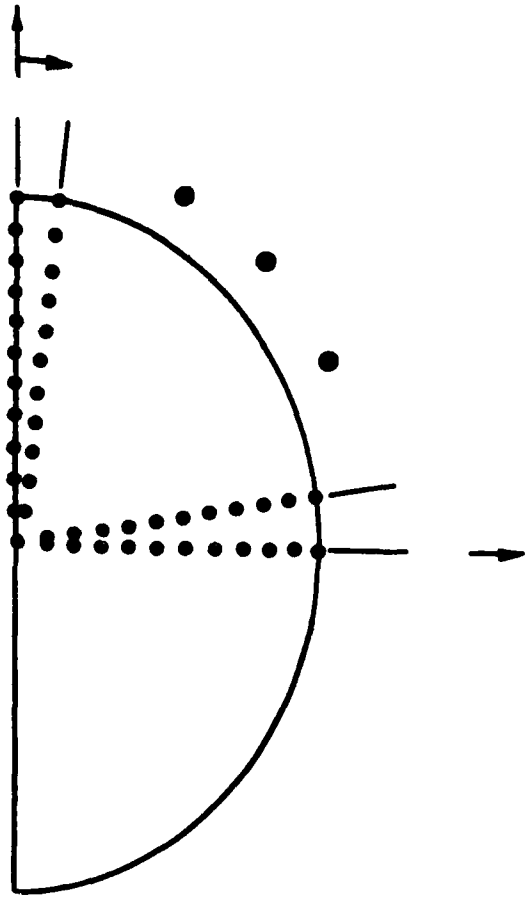

Figure C-1. Program COD Output Points

*U.S.Government Printing Office: 1981 — 559-006/5023